Srs2 binding to PCNA and its sumoylation contribute to RPA antagonism during the DNA damage response

Jiayi Fan[1], Nalini Dhingra[1#], Tammy Yang[2], Vicki Yang[2], Xiaolan Zhao[1]

[1]Molecular Biology Program, Memorial Sloan Kettering Cancer Center, New York, NY 10065

[2]City University of New York Hunter College, New York, NY 10065

Current address: Yale Center for Molecular Discovery, Yale University, West Haven, CT 06516

Corresponding author email: zhaox1@mskcc.org

Key words: DNA damage checkpoint, checkpoint dampening, Srs2, RPA, sumoylation, PCNA

Abstract

Activation of the DNA damage checkpoint upon genotoxin treatment induces a multitude of cellular changes, such as cell cycle arrest, to cope with genome stress. After prolonged genotoxin treatment, the checkpoint can be downregulated to allow cell cycle and growth resumption. In yeast, downregulation of the DNA damage checkpoint requires the Srs2 DNA helicase, which removes the ssDNA binding complex RPA and the associated Mec1 checkpoint kinase from DNA, thus dampening Mec1 activation. However, it is unclear whether the 'anti-checkpoint' role of Srs2 is temporally and spatially regulated to both allow timely checkpoint termination and to prevent superfluous RPA removal. Here we address this question by examining regulatory elements of Srs2, including its phosphorylation, sumoylation, and protein-interaction sites. Our genetic analyses and checkpoint level assessment suggest that the RPA countering role of Srs2 is promoted by Srs2 binding to PCNA, which is known to recruit Srs2 to subsets of ssDNA regions. RPA antagonism is further fostered by Srs2 sumoylation, which we found depends on the Srs2-PCNA interaction. Srs2 sumoylation is additionally reliant on Mec1 and peaks after Mec1 activity reaches maximal levels. Collectively, our data provide evidence for a two-step model wherein checkpoint downregulation is facilitated by PCNA-mediated Srs2 recruitment to ssDNA-RPA filaments and the subsequent Srs2 sumoylation stimulated upon Mec1 hyperactivation. We propose that this mechanism can allow Mec1 hyper-activation to trigger checkpoint recovery.

Introduction

The DNA damage response promotes organismal survival of genotoxic stress by eliciting many cellular changes. This includes a critical signaling process termed the DNA damage checkpoint (DDC). Upon encountering stress, the apical DDC kinases are recruited to DNA lesion sites by the damage sensing proteins and are then activated by activator proteins(Lanz, Dibitetto, & Smolka, 2019). A universal DDC sensor is the RPA complex that binds with high affinity and specificity to single-strand DNA (ssDNA), the abundancy of which rises under almost all types of genotoxic stress(Maréchal & Zou, 2015). Using the budding yeast as an example, RPA bound to the ssDNA filament can interact with Ddc2, the co-factor of the Mec1 checkpoint kinase, and recruit the Mec1-Ddc2 complex to DNA lesion sites. Subsequently, Mec1 is activated and can phosphorylate multiple substrates. Among these is a key downstream effector kinase Rad53, the phosphorylation of which turns on its own kinase activity and yields further phosphorylation. Collectively, the DDC kinases can modify hundreds of proteins, inducing multitudes of pathway changes (Lanz, Dibitetto, & Smolka, 2019) . For example, DDC can arrest the cell cycle progression to allow more time for genome repair, which is required for cellular survival (Sanchez et al., 1999; Wang et al., 2001).

While DDC activation is crucial for the cell to cope with genotoxic stress, its timely downregulation is equally vital (Waterman, Haber, & Smolka, 2020). Many changes induced by the DDC kinases need to be reversed to allow continued cell growth and recovery. For example, the DDC-mediated cell cycle arrest has to be lifted to allow proliferation and alternative DNA repair permitted at other cell cycle phases (Pellicioli et al., 2001; Waterman, Haber, & Smolka, 2020). Thus far, DDC downregulation has been mainly elucidated using the model organism yeast, with several strategies being identified (Waterman, Haber, & Smolka, 2020). One of these is mediated by the DNA helicase Srs2 that targets the most upstream step of the DDC pathway through removing RPA and the associated Mec1-Ddc2 from chromatin (Dhingra et al., 2021). The DDC dampening (anti-checkpoint) function of Srs2 was shown to be separable from its roles in removing the recombinase Rad51 from ssDNA (anti-recombination) during homologous recombination (Dhingra et al., 2021). Considering that other organisms also possess DNA helicases capable of removing RPA from ssDNA (Hormeno et al., 2022; Jenkins et al., 2021; Shorrocks et al., 2021), it is plausible that an anti-checkpoint strategy involving RPA antagonism may present beyond yeast.

Currently, little is known about how checkpoint dampening can be temporally controlled to minimize interference with the initial DDC activation that must occur in the early phase of the DNA damage response. In the case of the Srs2-mediated checkpoint regulation, it is also unclear how the process can minimize superfluous removal of RPA from sites of other RPA-mediated processes, such as at ongoing replication forks and transcription bubbles. In addressing these questions, we hypothesize that Srs2-based RPA antagonism should be selective in location and timing, and that the regulatory elements within the Srs2 protein may contribution to the selectivity.

To test the above hypothesis and to define Srs2 features relevant to its RPA antagonism during DDC regulation, we examined six Srs2 protein sites involved in its post-translational modifications and interactions with other proteins. Our genetic analyses of mutations affecting each of these sites suggest that while most of the examined features do not affect RPA antagonism, Srs2 binding to PCNA, which marks the 3' junction of ssDNA gaps, and Srs2 sumoylation contribute to RPA regulation in the context of DDC. Srs2 binding to PCNA was known to recruit Srs2 to replication perturbation sites, while the roles of Srs2 sumoylation were less studied but can affect rDNA recombination (Kolesar et al., 2012; Moldovan, Pfander, &

Jentsch, 2007; Papouli et al., 2005; Pfander et al., 2005; Saponaro et al., 2010). Unexpectedly, we found that Srs2 PCNA binding and its sumoylation are functionally related, as Srs2 binding to PCNA promotes its sumoylation. Moreover, Srs2 sumoylation level peaks late in the response to genomic stress after the DDC kinases are hyper-activated, and this modification depends on Mec1. Collectively, our data support a model wherein Srs2 recruitment to DNA lesion sites via binding to PCNA and subsequent sumoylation in a Mec1-dependent manner help to counter RPA functions and the Mec1 checkpoint.

Results

Srs2 regulatory features and their disabling mutants

To understand which Srs2 attributes are relevant to RPA regulation during the DNA damage response, we examined mutant alleles that perturb known features of the Srs2 protein. Srs2 was reported to contain a helicase domain at its N-terminal region and three protein-protein interaction sites at its C-terminal region (Fig.1A) (Niu & Klein, 2017). We have previously shown that the Srs2 ATPase-dead allele (*srs2-K41A*) fails to downregulate RPA and Mec1-mediated DDC, indicating a requirement of ATPase-driven stripping of RPA from ssDNA (Dhingra et al., 2021) . The reported Srs2 protein-bindings sites include a Rad51 binding domain (Rad51-BD), a PCNA interaction motif (PIM), and a SUMO interaction motif (SIM) (Fig. 1A) (Colavito et al., 2009; Kolesar et al., 2016; Kolesar et al., 2012). We used CRISPR-based editing to generate the *srs2-ΔPIM* (Δ1159-*11*63 a. a.) and the *srs2-SIMmut* ($_{1170}$ IIVID $_{1173}$ to $_{1170}$ AAAAD $_{1173}$) alleles based on previous reports and examined an established *srs2-ΔRad51BD* allele (Δ875-902 a.a.) (Colavito et al., 2009; Kolesar et al., 2016; Kolesar et al., 2012). We note that despite Srs2 removal of RPA from ssDNA, an interaction between the two proteins has not been reported.

We also queried post-translational modifications reported for Srs2 by mutating the corresponding modification sites (Fig. 1A). First, seven Cdk1 phosphorylation consensus sites of Srs2 were mutated to produce the *srs2-7AV* (T604V, S698A, S879A, S893A, S938A, S950A, and S965A) allele (Chiolo et al., 2005), which was previously shown to affect recombinational repair. Second, three sumoylation sites of Srs2 were mutated to generate *srs2-3KR* (K1081R, K1089R, and K1142R) (Saponaro et al., 2010). Finally, we mutated two serine residues (S890 and S933) to alanine to generate *srs2-2SA*, since phosphorylation at these sites was shown in proteomic studies as dependent on Mec1 and genotoxic treatments (Faca et al., 2020). Because the Srs2 C-terminal end contributes to protein functions (Antony et al., 2009; Colavito et al., 2009), the six mutant alleles described above were not tagged with epitopes. Using an anti-Srs2 specific antibody, we showed that all six alleles supported wild-type levels of Srs2 protein based on immunoblotting (Fig. 1B).

Mutating PCNA binding and sumoylation sites of Srs2 rescues *rfa1-zm2* CPT sensitivity

Srs2 loss leads to persistent DDC and perturbed recombination, both of which contribute to *srs2*Δ sensitivity to genotoxins, including camptothecin (CPT) that traps Top1 on DNA and methyl methanesulfonate (MMS) that methylates DNA (Fig. 2A) (Niu & Klein, 2017). Significantly, our recent study has showed that RPA mutants that reduce its ssDNA binding affinity can rescue the persistent DDC levels in *srs2*Δ cells but not their recombination defects (Dhingra et al., 2021). *rfa1-zm2* (N492D, K493R, K494R) is one of the RPA alleles examined that contains mutations at three DNA contacting residues in the Rfa1 subunit of RPA (Fan & Pavletich, 2012). A RPA variant complex with these mutations exhibits a two-fold increase in

dissociation constant compared to wild type RPA (Dhingra et al., 2021). In cells, *rfa1-zm2* supports normal Rfa1 protein level, cell growth, DNA replication, and recombinational repair (Dhingra et al., 2021). However, *rfa1-zm2* and *srs2*Δ are mutually suppressive for genotoxic sensitivities and DDC abnormalities (Fig. 2B, S1A) (Dhingra et al., 2021). These data suggest that the *srs2* and *rfa1-zm2* genetic relationship can be used as a readout for the antagonism between Srs2 and RPA during the DNA damage response. Based on this rationale, we employed the genetic suppression as an initial readout in querying whether any of the six *srs2* mutant alleles described above are related to RPA regulation. Given that Srs2's role in DDC dampening was best examined in CPT (Dhingra et al., 2021), experiments were mostly carried out in this condition.

We found that on their own, *srs2-SIM*^{mut}, -Δ*PIM*, and *-7AV* showed different levels of sensitivity toward CPT at a concentration ranging from 2 to 8 µg/ml, while *srs2-*Δ*Rad51BD* and *-3KR* exhibited close to wild-type level of CPT resistance, which are consistent with previous reports (Colavito et al., 2009; Saponaro et al., 2010) (Fig. S1A). In addition, *srs2-2SA,* which has not been examined previously*,* did not show CPT sensitivity (Fig. S1A). Since *rfa1-zm2* cells exhibited stronger CPT sensitivity than the tested *srs2* alleles (Fig. S1A), we asked if the latter could suppress *rfa1-zm2* CPT sensitivity. We found that both *srs2-*Δ*PIM* and *-3KR* improved the CPT resistance of *rfa1-zm2* cells on media containing 2 ug/ml CPT (Fig. 2C). Rescue was also seen at higher CPT concentrations, with *srs2-*Δ*PIM* exhibiting a stronger effect than *srs2-3KR* (Fig. S1B). In contrast to *srs2-*Δ*PIM* and *srs2-3KR*, *srs2-*Δ*Rad51BD* and -2SA showed no effect on *rfa1-zm2* growth on media containing CPT, whereas *srs2*-7AV *and -SIM*^{mut} worsened it (Fig. 2D). The differential effects seen for the *srs2* alleles are consistent with the notion that Srs2 has multiple roles in cellular survival of genotoxic stress (Bronstein et al., 2018; Niu & Klein, 2017). The unique suppression seen for mutants affecting Srs2 binding to PCNA and its sumoylation suggests that these features are relevant to RPA regulation during the DNA damage response.

Additional suppressive effects conferred by *srs2-*Δ*PIM* and *-3KR* toward *rfa1* mutants

We next tested whether the observed *srs2-*Δ*PIM* and *-3KR* suppression was specific towards *rfa1-zm2* or applicable to other *rfa1* mutants that are also defective in ssDNA binding. While *rfa1-zm2* affects the ssDNA binding domain C (DBD-C) of Rfa1, a widely used *rfa1* allele, *rfa1-t33,* impairs the DBD-B domain (Fig. 2E) (Umezu et al., 1998). Unlike *rfa1-zm2, rfa1-t33* additionally decreases Rfa1 protein level and interferes with DNA replication and repair (Deng et al., 2014; Umezu et al., 1998). Despite having these additional defects, CPT survival of *rfa1-t33* cells was also improved by *srs2-*Δ*PIM* or *srs2-3KR* (Fig. 2E). As seen in the case of *rfa1-zm2*, *srs2-*Δ*PIM* conferred better rescue than *srs2-3KR* toward *rfa1-t33* (Fig. 2E). When comparing the two *rfa1* alleles, *srs2* rescue was stronger toward *rfa1-zm2*, likely because *rfa1-t33* has other defects besides reduced ssDNA binding (Fig. 2C, 2E). In either case, *srs2* mutants only conferred partial suppression, consistent with the notion that Srs2 has roles beyond RPA regulation (Bronstein et al., 2018; Niu & Klein, 2017). Nevertheless, the observed rescue indicates that Srs2 PCNA binding and sumoylation are likely involved the regulation of RPA during the DNA damage response.

Srs2 regulation of RPA during DDC downregulation is not only observed under CPT treatment, but also in MMS treatment, conditions (Dhingra et al., 2021). Consistent with this observation, *srs2-*Δ*PIM* moderately improved MMS sensitivity of *rfa1-zm2* and *rfa1-t33,* while *srs2-3KR* had a small effect on the MMS sensitivity of *rfa1-zm2* (Fig. S1B, S1C). Collectively*,*

the genetic results provide evidence that the roles of Srs2 binding to PCNA and sumoylation in RPA antagonism can be applicable to more than one genomic stress situations.

srs2-ΔPIM and *-3KR* rescue checkpoint abnormality of *rfa1-zm2* cells

We next investigated whether *srs2-ΔPIM* and *-3KR* suppression of *rfa1-zm2* pertained to DNA damage checkpoint regulation. We employed two readouts for DDC, including the levels of the phosphorylated and active form of Rad53 detectable by the F9 antibody (Fiorani et al., 2008) and cellular ability to exit the G2/M phase after CPT treatment. We have previously shown that *srs2Δ* cells exhibit increased levels of Rad53 phosphorylation and diminished ability to exit G2/M phase in CPT, and that both are suppressed by *rfa1-zm2* (Dhingra et al., 2021). Interestingly, *rfa1-zm2* leads to similar defects and these are rescued by *srs2Δ* (Dhingra et al., 2021). The mutual suppression seen in these assays is consistent with that seen for CPT sensitivity (Dhingra et al., 2021). We note that several other RPA ssDNA binding mutants, such as *rfa1-t33*, also exhibit phenotypes indicative of increased DDC levels (Pellicioli et al., 2001; Seeber et al., 2016; Smith & Rothstein, 1995; Zou & Elledge, 2003). This is likely because compromised ssDNA protection can lead to increased levels of DNA lesions thus enhancing the activation of Mec1 and/or its homolog Tel1.

We reasoned that if *srs2-ΔPIM* and *srs2-3KR* compromise Srs2's ability to remove RPA from DNA in cells, they should alleviate *rfa1-zm2* cells' defects in ssDNA protection and the associated DDC abnormalities. Indeed, while *rfa1-zm2* exhibited about 5-fold increase in Rad53 phosphorylation levels in CPT compared with wild-type cells as seen before (Dhingra et al., 2021), *srs2-ΔPIM* and *-3KR* reduced this level by about 50% and 80%, respectively (Fig. 3A). Similar to earlier data, we observed that wild-type cells arrested in G_2/M after 1 hour of CPT treatment and ~25% of these cells entered G_1 after another hour (Fig. 3B) (Dhingra et al., 2021). The ability to exit from G_2/M phase was reduced in *rfa1-zm2* cells so that only 13% cells moved to G1 phase after 2 h treatment with CPT, as seen before (Fig. 3B) (Dhingra et al., 2021). Significantly, *srs2-ΔPIM* and *-3KR* allowed increased the percentage of *rfa1-zm2* cells to transit into G1 phase (Fig. 3B). The suppressive effects seen in both assays was stronger for *srs2-ΔPIM* than *srs2-3KR* as seen in genotoxicity assays (Fig. S1B; 3A, 3B). Collectively, the genetic and DDC assay data are consistent with each other and suggest that Srs2 binding to PCNA and its sumoylation contribute to RPA antagonism in DDC regulation.

srs2-ΔPIM is additive with a *slx4* mutant defective in DDC recovery

We found that *srs2-ΔPIM* and *srs2-3KR* mutants on their own behaved normally in the two DDC assays described above, which differs from *srs2Δ* cells that exhibit increased levels of Rad53 phosphorylation and reduced G1 entry (Fig. 3A, 3B) (Dhingra et al., 2021). One plausible interpretation of this difference is that unlike *srs2Δ*, these partial *srs2* mutants only mildly impair Srs2-mediated RPA regulation during DDC downregulation, such that their defects can be compensated for by other DDC dampening systems. To test this idea, we examined the consequences of removing the Slx4-mediated anti-checkpoint function in *srs2-ΔPIM* cells. Slx4 is known to bind the scaffold protein Rtt107, and their complex can compete with the DDC protein Rad9 for binding to damaged chromatin, consequently disfavoring Rad9's role in promoting Rad53 phosphorylation (Ohouo et al., 2013). Slx4 uses an Rtt107 interaction motif (RIM) to bind Rtt107 and a previously established RIM mutant, $slx4^{RIM}$ (T423A, T424A, and S567A), abolishes Rtt107 binding without affecting other Slx4 protein attributes (Wan et al., 2019). $slx4^{RIM}$ was tagged with a TAP tag at its C-terminal end and examined together with a

control wherein the wild-type Slx4 was tagged in the same manner. Compared with the control. *slx4*^{RIM} exhibited mild sensitivity toward CPT (Fig. S2A). Significantly, when *srs2-ΔPIM* was combined with *slx4*^{RIM}, the double mutant exhibited stronger CPT sensitivity compared with corresponding single mutants (Fig. S2A).

We further examined DDC levels when cells were exposed to CPT using both Rad53 phosphorylation and ability to exit G2/M as readouts. Compared with *SLX4-TAP* cells, *slx4*^{RIM}*-TAP* cells exhibited 2-fold increase in Rad53 phosphorylation level, consistent with a role of Slx4-RIM in downregulating DDC (Fig. S2B). In *SLX4-TAP* background, *srs2-ΔPIM* led to 3-fold increase in Rad53 phosphorylation level (Fig. S2B). As cells containing untagged Slx4 and *srs2-ΔPIM* did not show Rad53 phosphorylation changes (Fig. 3A), tagging Slx4 likely sensitizes *srs2-ΔPIM.* Significantly, the double mutant of *srs2-ΔPIM* and *slx4*^{RIM}*-TAP* exhibited further increase in Rad53 phosphorylation (~5.5 fold) compared with *srs2-ΔPIM* and *slx4*^{RIM}*-TAP* single mutant (Fig. S2B). Congruous with this finding, the *srs2-ΔPIM slx4*^{RIM}*-TAP* double mutant also reduced the percentage of cells entering G_1 from G2/M arrest compared with their single mutants (Fig. S2C). Together, these three lines of evidence support the notion that defects in the Srs2-mediated DDC downregulation can be compensated for by Slx4-mediated mechanisms.

Srs2 binding to PCNA facilitates Srs2 sumoylation

We next addressed whether the two Srs2 features involved in RPA antagonism are functionally related. To this end, we tested if Srs2 binding to PCNA affected Srs2 sumoylation in cells. We confirmed that endogenous sumoylation of Srs2 could be detected in cell extracts after enriching SUMOylated proteins using 8His-tagged SUMO (8His-Smt3) (Fig. 4A). Briefly, proteins were extracted from cells under denaturing conditions to disrupt protein-protein association and prevent desumoylation, and sumoylated proteins were enriched on Ni-NTA (nickel-nitrilotriacetic acid) resin (Ulrich & Davies, 2009). Consistent with previous findings, sumoylated forms of Srs2 in the Ni-NTA elute were detected on immunoblots using an anti-Srs2 antibody only when cells contained 8His-Smt3, where unmodified Srs2 was seen regardless of the presence or absence of 8His-Smt3 due to nonspecific binding to the resin (Fig. 4A) (Saponaro et al., 2010). These bands were only seen in wild-type cells but not *srs2Δ* cells (Fig. S3A). We found that Srs2 sumoylation level was reduced in *srs2-3KR* strains in CPT conditions, as expected from mutating the three major sumoylation sites (Fig. 4A) (Saponaro et al., 2010). Interestingly, *srs2-ΔPIM* cells exhibited a similar reduction of Srs2 sumoylation as seen in *srs2-3KR* cells (Fig. 4A). This result suggests that Srs2 sumoylation largely depends on Srs2 binding to PCNA, supporting the notion that the two events occur sequentially.

Srs2 sumoylation peaks after maximal Mec1 activation and depends on Mec1

While RPA can engage with ssDNA generated in different processes, such as transcription and replication, only a subset of ssDNA regions is adjacent to 3'-junction loaded PCNA. This is because PCNA loading occurs mainly during S phase and requires a ssDNA and dsDNA junction site permissive for loading (Moldovan, Pfander, & Jentsch, 2007). We thus reasoned that Srs2 binding to PCNA may prevent Srs2 from removing RPA bound to ssDNA that forms transiently or is not flanked by PCNA, such as within transcription bubbles, R-loop regions, or at ongoing replication forks. This could provide a means for spatial control of Srs2's anti-RPA role. We explored whether this role could also be regulated temporally. As the genetic data described

above suggest that Srs2 sumoylation acts downstream of Srs2 binding to PCNA in antagonizing RPA, we examined the timing of Srs2 sumoylation after CPT treatment.

We released G1 synchronized cells into media containing CPT and examined Srs2 sumoylation at several time points (Fig. 4B). A similar experimental scheme was used to monitor the level of Mec1 activation using Rad9 phosphorylation level as a readout (Fig. 4C). Quantification of Srs2 sumoylated forms relative to its unmodified forms showed that its sumoylation level peaked between 1.5 and 2 h after releasing cells into CPT (Fig. 4D). Quantification of phosphorylated forms of Rad9 relative to its unmodified form showed that checkpoint activation peaked 1 hour after cell release (Fig. 4D). That checkpoint level peaked before Srs2 sumoylation level peaked suggests a possible dependence of the latter on the checkpoint. In testing this idea, we found that *mec1*Δ cells, which contain *sml1*Δ to support viability, abolished Srs2 sumoylation (Fig. 4E). Neither *sml1*Δ alone nor removal of Rad53 affected Srs2 sumoylation (Fig. 4E), suggesting that Mec1's effect on this modification does not require the downstream Rad53 effector kinase. As Mec1 is not generally required for protein sumoylation during the DNA damage response (Cremona et al., 2012), its involvement in Srs2 sumoylation presents a rather unique effect.

Examination of Mec1-S1964 phosphorylation in Srs2-mediated DDC regulation

The combined results that Srs2 sumoylation levels peak after those of Rad9 phosphorylation and that Srs2 sumoylation depends on Mec1 raised the possibility that Mec1 hyper-activation during the late part of the DNA damage response may favor Srs2's role in DDC dampening. Recently, Mec1 protein bound to Ddc2 was shown to be auto-phosphorylated at Ser1964 in a late part of the DNA damage response after a single DNA break is induced by the HO endonuclease (Memisoglu et al., 2019). Further, the phosphorylation defective mutant *mec1-S1964A* impaired checkpoint downregulation in this condition, leading to the model that Mec1-S1964 phosphorylation contributes to DDC dampening at least after HO-induced break (Memisoglu et al., 2019). We tested the idea whether Mec1-S1964 phosphorylation is also involved in Srs2-mediated DDC regulation in CPT condition.

First, we asked whether Mec1-S1964 phosphorylation occurs in CPT condition using a time course scheme similar to the one used in testing Srs2 sumoylation. Ddc2-bound Mec1 was recovered after immunoprecipitating Ddc2 at each timepoint and the proteins were examined by immunoblotting. To detect Mec1-S1964 phosphorylation, we used an antibody raised against the peptide containing this modification (Memisoglu et al., 2019). The antibody detected the Mec1 S1964 phosphorylation band in immunoprecipitated fractions only when Ddc2 was tagged with the Myc tag but not when Ddc2 was untagged (Fig. S3B). Further, the Mec1 S1964 phosphorylation band was largely abolished in the *mec1-S1964A* cells. (Fig. S3B; 5A). Given that the antibody also detects a closely spaced background band (Fig. S3B; 5A), we calculated the relative level of Mec1 S1964 phosphorylation in each sample by normalizing to this band. Quantification results showed that Mec1 S1964 phosphorylation level peaked around the same time as seen for Rad9 phosphorylation, which is 1 hour after CPT treatment (Fig. 5A).

After confirming that Mec1 S1964 phosphorylation also took place in CPT conditions, we tested whether *mec1-S1964A* or the phosphorylation mimetic mutant *mec1-S1964E* influenced *rfa1-zm2* or *srs2* growth on media containing CPT. If Mec1 S1964 phosphorylation aids Srs2-mediated RPA antagonism in CPT, we would expect *mec1-S1964A* to behave like *srs2* mutants in rescuing *rfa1-zm2* CPT sensitivity, while *mec1-S1964E* should have the opposite effects. We found that *mec1-S1964A,* which showed normal CPT resistance on its own, did not affect *rfa1-*

zm2 cell growth on CPT (Fig. 5B). *mec1-S1964A* also did not influence the growth of *srs2-ΔPIM* and *srs2-3KR* cells regardless of *rfa1-zm2* (Fig. 5B, S5A).

Though *mec1-S1964E* on its own did not cause no CPT sensitivity, it led to slight but reproducible slow growth in cells containing *srs2-3KR* and *srs2-ΔPIM* with or without *rfa1-zm2* (Fig. S4B). We found that neither *mec1-S1964A* nor *mec1-S1964E* affected Srs2 sumoylation levels (Fig. S4C). Thus, Mec1, but not its S1964 phosphorylation, is required for Srs2 sumoylation. These data provide evidence that even though an HO-induced DNA break and CPT treatment both induce Mec1 S1964 phosphorylation, this modification appears to not affect Srs2-mediated DDC dampening in the former situation.

Genetic data suggest that known RPA phosphorylation sites do not affect DDC recovery

While we mainly focused on the identification of Srs2 features that contribute to RPA antagonism during DDC regulation, we also considered the possibility that certain regulatory RPA features may contribute to this regulation as well. In particular, RPA is known to be phosphorylated by Mec1 (Chen et al., 2010; Faca et al., 2020; Lanz et al., 2021). We thus tested the idea that this may render RPA more susceptible to be removed from ssDNA by Srs2. To this end, we mutated previously identified Mec1 phosphorylation sites on the Rfa1 and Rfa2 subunits. These include Rfa1 Ser178 and three sites on Rfa2 (S122, S187, S189) (Albuquerque et al., 2015; Chen et al., 2010). We generated corresponding non-phosphorylatable mutants, *rfa1-S178A* and *rfa2-3SA (*S122A, S187A, and S189A), and phosphomimetic mutants, *rfa1-S178D* and *rfa2-3SD*.

Using genetic suppression as a readout for possible involvement of RPA mutants in Srs2-based DDC regulation, we examined the interactions between these mutants and *srs2*Δ. If RPA phosphorylation can promote RPA removal by Srs2, the *SD* mutants may show suppressive interaction with *srs2*Δ, while *SA* mutants would behave like *srs2* mutants. We found that *rfa1-S178D* nor *S178A*, which on their own both showed normal CPT resistance, did not affect *srs2*Δ cell growth on CPT-containing media (Fig. 5C). In contrast, *rfa2-3SD* or *rfa2-3SA,* which also behaved like wild-type regarding CPT sensitivity, sensitized *srs2*Δ growth on CPT-containing media (Fig. 5D). This negative genetic interaction is in contrast to the positive interaction seen between *srs2*Δ and *rfa1-zm2* or *rfa1-t33* (Fig. S1A) (Dhingra et al., 2021). The differential Srs2 genetic interactions among distinct RPA alleles likely reflects the multi-functional natures of Srs2 and RPA. Collectively, these analyses suggest that known phosphorylation sites on RPA are unlikely involved in the Srs2-based DDC regulation.

Discussion

Timely termination of DDC is crucial for cell survival, yet the underlying mechanisms are not well understood. Using the budding yeast model system, we investigated how the Srs2-mediated DDC downregulation through antagonizing RPA can be regulated. Our previous work reports a requirement of Srs2's ATPase activity in this role; here we examined six additional Srs2 features involved in either binding to other proteins or post-translational modifications. Our results suggest that among the examined features, only Srs2 binding to PCNA and its sumoylation are involved in RPA antagonism during DDC downregulation. Interestingly, these two features are functionally linked, as Srs2 binding to PCNA is required for optimal Srs2 sumoylation. Further, Srs2 sumoylation level peaks after Mec1 activity reaches its maximal level and that Mec1 is

required for this modification. We posit a model that can interpret both previous and current data (Fig. 6). We envision that Srs2 binding to PCNA that is loaded at the 3' junction site flanking ssDNA gaps can help to bring Srs2 in proximity to the RPA-ssDNA filament and promote Srs2 sumoylation, both favoring downregulation of the checkpoint (Fig. 6). These regulatory mechanisms could in principle help to minimize undesirable RPA loss from PCNA-free regions and premature RPA removal from DNA during checkpoint induction phase.

Our initial assessment of six Srs2 mutants used genetic suppression of the *rfa1-zm2* CPT sensitivity as a readout for Srs2 and RPA antagonism. The results suggest that RPA regulation involves Srs2 binding to PCNA and Srs2 sumoylation, but not Srs2 binding to either Rad51 or SUMO nor its phosphorylation at Cdk1 sites and two potential Mec1 kinase sites. Genetic analysis showed that the suppression conferred by mutating PCNA binding sites on Srs2 (*srs2*Δ*-PIM*) in *rfa1-zm2* cells also extended to MMS conditions. Additionally, a similar suppression for another *rfa1* mutant defective in ssDNA binding was seen. These results ruled out suppression being specific to one allele or one genotoxin. Data from two checkpoint assays further showed that *srs2*Δ*-PIM* and *srs2-3KR* suppressed DDC abnormalities in *rfa1-zm2* cells, strengthening the conclusion that Srs2 binding to PCNA and its sumoylation help to counter RPA during the DNA damage response.

RPA coats ssDNA generated from many DNA metabolic processes; thus, selective RPA stripping can be beneficial in cells. Our data suggest that this selectivity could be partially achieved by Srs2 binding to PCNA. In principle, ssDNA regions not adjacent to stable 3' ss-dsDNA junction sites, such as those formed during transcription and in the R-loop regions, could be spared from Srs2-mediated RPA stripping. In contrast, ssDNA regions adjacent to PCNA-loaded junction sites, such as at ssDNA gap regions behind the replication forks, can be better targeted for Srs2-mediated RPA removal. An involvement of PCNA binding in Srs2-based RPA regulation could also compensate for a lack of Srs2 interaction with RPA. This scenario differs from Srs2-based Rad51 stripping that requires their interaction (Antony et al., 2009; Colavito et al., 2009; Krejci et al., 2003). It is thus likely that though both the anti-recombinase and anti-checkpoint roles of Srs2 can benefit from selectivity, they are achieved via different means. Previous studies have suggested that both PIM and SIM aid Srs2 recruitment to sumoylated form of PCNA (Papouli et al., 2005; Pfander et al., 2005). Our data reveal that at least in CPT conditions, Srs2-PIM, but not Srs2-SIM, is involved in RPA regulation. This observation is congruent with phenotypic differences between Srs2's PIM and SIM seen in other studies and here, such as much stronger genotoxic sensitivity of the latter (Fig. S1A) (Fan et al., 2023; Kolesar et al., 2016; Kolesar et al., 2012). Considering that only a small percentage of PCNA is sumoylated and mainly during S phase (Papouli et al., 2005; Pfander et al., 2005), it is probably advantageous for Srs2 not being restricted to sumoylated PCNA for efficient RPA regulation.

How could Srs2 binding to PCNA helps Srs2 sumoylation? While a full answer awaits future studies, we speculate that this interaction may render Srs2 more permissive for sumoylation and/or position Srs2 in proximity with its sumoylation E3 ligase Siz2 that binds RPA (Chung & Zhao, 2015; Kolesar et al., 2012). Considering that Mec1, Ddc2, and RPA contain SUMO interaction motifs (Psakhye & Jentsch, 2012), it is possible that Srs2 sumoylation could help enrich the helicase at ssDNA-RPA sites via interacting with these motifs, though other effects are also possible. Compared with *srs2-3KR*, *srs2-*Δ*PIM* showed better suppression of *rfa1-zm2* defects. This indicates that during RPA regulation, PCNA plays additional roles besides promoting Srs2 sumoylation.

We found that Srs2 sumoylation in cells also requires Mec1, which does not promote sumoylation in general (Cremona et al., 2012). On the contrary, Mec1 loss causes increased

sumoylation levels (Cremona et al., 2012). It is currently unclear how Mec1 can specifically promote Srs2 sumoylation, but this may involve Mec1-mediated phosphorylation of SUMO substrates and/or enzymes. A requirement of Mec1 for Srs2 sumoylation and the dynamic nature of sumoylation suggest that Srs2 sumoylation may be a potential timing regulator. It is possible that hyperactivation of Mec1 favors Srs2 sumoylation that may aid its own downregulation. While fully testing this idea requires time-course phosphoproteomic studies under genotoxin treatment, we examined a Mec1 auto-phosphorylation site implicated in its downregulation after induction of a single DNA break (Memisoglu et al., 2019). We did not find evidence that this is involved in Mec1 dampening in CPT condition, raising the possibility that distinct mechanisms may be used in different genomic stress conditions. We also found that two phosphorylation sites on Srs2 that showed Mec1 dependency in proteomic studies had no effect in the CPT situation (Albuquerque et al., 2015; Faca et al., 2020); however we note that these sites do not fit with the typical S/TQ Mec1 consensus sites, thus may not be the bona fide Mec1 sites. Other phosphorylation sites examined here include five Mec1 sites on Rfa1 and Rfa2 (Albuquerque et al., 2015; Chen et al., 2010). Genetic analyses did not support their roles in the Srs2 and RPA antagonism. Thus, future studies to comprehensively map DDC kinase phosphorylation sites on Srs2 and RPA, as well as their regulators, such as the RPA chaperone Rtt105 (Li et al., 2018), will be needed to test how the kinases can communicate with Srs2-based RPA regulation during the DNA damage response.

While we provide multiple lines of evidence in support of the involvement of Srs2 binding to PCNA and its sumoylation in RPA regulation during checkpoint downregulation, *srs2-ΔPIM* or *-3KR* alone behaved normally in checkpoint assays. The lack of a defect here can be due to buffering effects, both from not-yet characterized Srs2 features and from other checkpoint dampening pathways. We provided evidence for the latter since *srs2-ΔPIM* or *-3KR* showed additive phenotype when combined with a *slx4* mutant defective in DDC dampening function. The presence of multiple checkpoint dampening factors that target different checkpoint modules highlights the importance of the process. Recent demonstration of other DNA helicases, such as the human HELB, HELQ, and BLM proteins, in stripping of RPA from ssDNA in vitro suggests that Srs2-like checkpoint downregulation may present in human cells as well (Hormeno et al., 2022; Jenkins et al., 2021; Shorrocks et al., 2021). Since RPA-ssDNA binding not only plays a key role in checkpoint, but also in many other processes, the Srs2 features uncovered here may help to better understand how RPA dynamics is controlled by helicases and other factors during additional processes beyond DDC.

Methods

Yeast strains and genetic techniques. Standard procedures were used for cell growth and media preparation. Strains used in this work are listed in Table S1; they are isogenic to W1588-4C, a *RAD5* derivative of W303 (Zhao & Blobel, 2005). Mutant alleles of *srs2*, *rfa1*, *rfa2, mec1* used in this work were generated by CRISPR-Cas9 based gene replacement, except for *srs2-3KR* that was introduced using a PCR-based method (DiCarlo et al., 2013). All mutations were verified by sequencing. Standard procedures were used for tetrad analyses and genotoxin testing. For each assay, at least two biological duplicates were used per each genotype. Cells were grown at 30 ºC unless otherwise stated.

Cell synchronization and cell cycle analyses. Cells from log-phase cultures were treated with 5 μg/mL α factor (GenScript RP01002) for 1 h, followed by an additional 2.5 μg/mL α factor for 30 min. When at least 95% cells were arrested in G1 phase based on the percentages of unbudded cells, cells were released into yeast extract–peptone–dextrose (YPD) media

containing 100 µg/mL Protease (Millipore 53702) and 16 µg/mL CPT (Sigma C9911) for 2 h. Cell cycle progression was monitored by standard flow cytometry analyses as described previously (Zhao & Rothstein, 2002).

Protein extraction using trichloroacetic acid (TCA). To examine Srs2 levels, the active form of Rad53, and Rad9 phosphorylation, cell extracts were prepared as reported (Regan-Mochrie et al., 2022) . Briefly, 2×10^8 cells were collected at indicated time points. Cell pellets were resuspended in 20% TCA and lysed by glass bead beating. The lysate was centrifuged to remove supernatant. Precipitated proteins were suspended in Laemmli buffer (65 mM Tris-HCl at pH 6.8, 2% SDS, 5% 2-mercaptoethanol, 10% glycerol, 0.025% bromophenol blue) with 2 M Tris to neutralize the solution. Prior to loading, samples were boiled for 5 min and spun down at 14,000 rpm for 10 min to remove insoluble materials. Samples were separated on 4-20% Tris-glycine gels (Bio-Rad 456-1096) to examine Srs2 level and active Rad53 form or 7% Tris-acetate gels (Thermo Fisher EA03555) to detect Rad9 phosphorylation.

Detection of Srs2 sumoylation. Sumoylated proteins were pulled down from cells containing 8His-tagged SUMO expressed from its endogenous locus using standard Ni-NTA pull-down method as previously described (Ulrich & Davies, 2009). Briefly, protein extracts prepared in 55% TCA were incubated in buffer A (6 M guanidine HCl, 100 mM sodium phosphate at pH 8.0, 10 mM Tris-HCl at pH 8.0) with rotation for 1 h at room temperature. The cleared supernatant was obtained after centrifugation for 20 min and was then incubated with Ni-NTA resin (Qiagen 30210) in the presence of 0.05% Tween-20 and 4.4 mM imidazole overnight at room temperature with rotation. Beads were washed twice with buffer A supplemented with 0.05% Tween 20 and then four times with buffer C (8 M urea, 100 nM sodium phosphate at pH 6.3, 10 mM Tris-HCl at pH 6.3) supplemented with 0.05% Tween 20. HU buffer (8 M urea, 200 mM Tris-HCl at pH 6.8, 1 mM EDTA, 5% SDS, 0.1% bromophenol blue, 1.5% DTT, 200 mM imidazole) was used to elute proteins from the beads. Samples were loaded on NuPAGE™ 3–8% Tris-acetate gels (Thermo Fisher EA03752) followed by immunoblotting to detect both sumoylated and unmodified Srs2. Ponceau S stain was used to ensure equal loading.

Detection of Mec1 S1964 phosphorylation during CPT treatment. G1 arrested cells were filtered and resuspended in prewarmed YPD media containing 16 µg/mL CPT to allow entry into S phase. Samples are collected at indicated time points. Cells were disrupted by glass bead beating in lysis buffer before centrifugation for 15 min at 20,000 g to obtain whole-cell extract. The lysis buffer contains 25 mM K-HEPES (pH 7.6), 100 mM NaCl, 100 mM K-glutamate, 5 mM $Mg(OAc)_2$, 0.02% NP40, and 0.5% Triton X-100 supplemented by protease inhibitor cocktail (Sigma P8215) and Complete Ultra EDTA-free protease inhibitor (Roche11836145001). The activated form of Mec1 was enriched by immunoprecipitating myc-tagged Ddc2 using Protein A beads and anti-Myc antibody (Thermo Fisher 9E10) for 2–4 h at 4°C. Beads were washed five to six times using lysis buffer, and proteins were eluted using Laemmli buffer (65 mM Tris-HCl at pH 6.8, 2% SDS, 5% 2-mercaptoethanol, 10% glycerol, 0.025% bromophenol blue). After boiling for 5 min, eluted proteins were loaded onto NuPAGE™ 3–8% Tris-acetate gels and subjected to SDS-PAGE and immunoblotting analyses.

Immunoblotting analysis and antibodies. After SDS-PAGE, proteins were transferred to a 0.2-µm nitrocellulose membrane (GE, #G5678144) for immunoblotting. Pgk1 was used as a loading control. Antibodies used were anti-myc (Thermo, Fisher 9E10). anti-Srs2 (Santa Cruz, yC-18), anti-Pgk1 (Invitrogen, 22C5D8), F9 (a kind gift from Marco Foiani and Daniele Piccini, The FIRC Institute of Molecular Oncology, Milan, Italy) (Pellicioli et al., 2001), anti-Rad9 (a kind gift from John Petrini, MSKCC, NY, USA) (Usui, Foster, & Petrini, 2009), anti-Mec1-S1964-p (a kind gift from James E. Haber, Brandeis University, MA, USA) (Memisoglu et al., 2019).

Validation of antibodies is provided either by the manufacturers or in the cited references. Membranes were scanned with a Fujifilm LAS-3000 luminescent image analyzer, which has a linear dynamic range of 10^4. The signal intensities of nonsaturated bands were measured using ImageJ software. For graphs, data are shown as mean and SD. Statistical differences were determined using two-side Student's t tests.

Figure Legends.

Figure 1. Regulatory features of Srs2 and corresponding mutants.

(A) Schematic of Srs2 protein domains, regulatory features, and mutations affecting each of its features. Cdk1 phosphorylation sites depicted here include T604, S698, S879, S893, S938, S950, and S965 (Chiolo et al., 2005). Potential Mec1 phosphorylation sites include S890 and S933 (Albuquerque et al., 2015; Faca et al., 2020). Sumoylation sites mapped previously include K1081, K1089, and K1142 (Saponaro et al., 2010). Protein-interaction domains or motifs include the Rad51 binding domain (BD), PCNA Interaction Motif (PIM), and SUMO Interaction Motif (SIM) (Colavito et al., 2009; Kolesar et al., 2016; Kolesar et al., 2012). The residues for these domains are indicated. Mutant alleles disabling each of these features are included in the parentheses.

(B) Mutations affecting Srs2 features do not affect Srs2 protein level. Protein extracts were prepared from asynchronous cells. Srs2 was examined using anti-Srs2 antibody by immunoblotting. Srs2 levels in each mutant were first normalized to the Pgk1 loading control and then to those in wild-type cells. Mean of two biological isolates per genotype is graphed with error bars representing standard deviation (SD).

Figure 2. Srs2 PCNA binding and sumoylation are involved in suppressing *rfa1* mutants

(A) Schematic to show that Srs2's roles in checkpoint dampening (anti-checkpoint for simplicity) and DNA repair both contribute to genotoxin resistance.

(B) Schematic to highlight the mutual suppression between *srs2*Δ and *rfa1* mutants and the underlying effects on the RPA-ssDNA levels in cells.

(C) *srs2-*Δ*PIM* and *-3KR* suppress *rfa1-zm2* sensitivity to CPT. A 10-fold serial dilution of cells of the indicated genotypes were spotted and growth was assessed after incubation at 30°C for 40 hours unless otherwise noted.

(D) Several *srs2* mutants did not suppress *rfa1-zm2* sensitivity to CPT. Experiments were performed as in panel 2C.

(E) *srs2-*Δ*PIM* and *-3KR* suppress *rfa1-t33* sensitivity to CPT. Top: schematic of the Rfa1 protein domains and *rfa1* mutant alleles. Bottom: *srs2-*Δ*PIM* and *-3KR* improved *CPT* sensitivity of *rfa1-t33* cells. Experiments were performed as in panel 2C.

Figure 3. *srs2-*Δ*PIM* and *-3KR* correct checkpoint abnormalities in *rfa1-zm2* cells.

(A) *srs2-*Δ*PIM* and *-3KR* reduce the levels of active Rad53 in *rfa1-zm2* cells. Protein extracts were examined after G1 cells were released into cycling in the presence of 16 ug/ml CPT for 2 hours. Activated Rad53 was detected by the F9 antibody by immunoblotting. Active Rad53 signals in each indicated strain were compared to the Pgk1 loading control and normalized to those of *rfa1-zm2*. Two biological isolates per genotype were examined in two technical repeats and results are graphed with error bars representing SD. T-test generated *p* value is indicated.

(B) *srs2-*Δ*PIM* and *-3KR* allow better G1 entry of *rfa1-zm2* cells. Experiments were performed as in panel A and samples were collected at indicated time points. FACS profiles of the samples are shown at the top and percentages of G1 cells after 2 hours of CPT treatment (CPT 2 h) are plotted at the bottom. Two biological isolates per genotype were examined in two technique repeats and results are graphed with error bars representing SD. T-test generated *p* value is indicated.

Figure 4. Srs2 sumoylation depends on Srs2 PIM motif and the Mec1 kinase

(A) Srs2 sumoylation level is reduced in *srs2-ΔPIM* cells. Samples were collected after CPT treatment as in Figure 3A and sumoylated proteins were enriched as described in the text and methods. Sumoylated form of Srs2 (Srs2-Su) migrated slower than unmodified Srs2 on gel and both were detected using anti-Srs2 antibody in immunoblotting. Equal loading is indicated by Ponceau-S stain (Stain). The levels of sumoylated Srs2 relative to those of unmodified Srs2 were normalized to wild-type cells and plotted. Two biological isolates per genotype were examined in two technique repeats and results are graphed with error bars representing SD. T-test generated *p* value is indicated. ns, not significant.
(B) Srs2 sumoylation level during CPT treatment. Samples were collected as described in Figure 3B. Experiments were conducted, and immunoblotting data is presented as those in panel A. Time 0 samples are G1 cells before CPT treatment. FACS analysis at corresponding time points are included below the plot.
(C) Rad9 phosphorylation level during CPT treatment. Samples used in panel B were examined for Rad9 phosphorylation using an anti-Rad9 antibody. Unmodified and phosphorylated (Rad9-p) Rad9 forms are indicated. FACS analysis at corresponding time points are indicated below blots.
(D) Quantification of Srs2 sumoylation and Rad9 phosphorylation level changes during CPT treatment. Srs2 sumoylation signals were normalized based on unmodified form. Values at each timepoint were relative to that of G1 sample (Time 0) before CPT treatment, and fold changes were indicated on left y-axis. Rad9 signals were normalized to non-modified form and percentage of phosphorylated form were indicated on right y-axis. Two biological isolates per genotype were examined in two technique repeats and results are graphed with error bars representing SD.
(E) Mec1 is required for Srs2 sumoylation. Experiments were performed and data are presented as in panel A.

Figure 5. Mec1 and RPA phosphorylation did not link to Srs2 anti-checkpoint function.
(A) Mec1 autophosphorylation at S1964 during CPT treatment. Samples were collected as described in Figure 3B. Ddc2-myc was immunoprecipitated and the associated Mec1 was co-purified. The anti-Mec1-S1964-p antibody detected the phosphorylated form of Mec1 and a non-specific band (*). Quantification below the blot was based on results from two biological isolates.
(B) *mec1-S1964A* did not rescue *rfa1-zm2* sensitivity toward CPT. Experiments were performed as in Figure 2C.
(C) Examination of the *rfa1-S178A* and *-S178D* mutants. Top: schematic of the Rfa1 protein domains and position of Ser178. ssDNA binding domain (DBD) A-C are shown. Bottom, *rfa1-S178A* and *-S178D* had no effect on *srs2Δ*'s sensitivity to CPT. Experiments were performed as in Figure 2C.
(D) Examination of the *rfa2-3SA* and *-3SD* mutants. Top, schematic of the Rfa2 protein domains and position of Ser122, Ser187 and Ser189 mutated in *rfa2-3SA* and *-3SD*. ssDNA binding domain (DBD)-D is indicated. Bottom, *rfa2-3SA* has no effect on *srs2Δ*'s sensitivity toward CPT while *rfa2-3SD* showed additive effect. Experiments were performed as in Figure 2C.

Figure 6. A working model for the regulation of Srs2-mediated checkpoint dampening.
Genomic sites containing ssDNA gaps can be generated during disrupted DNA replication and DNA repair under genotoxin treatment. The resultant ssDNA gaps can be coated by RPA, which then recruit the Mec1/Ddc2 kinase complex. Mec1 is subsequently activated by DDC proteins, such as the 9-1-1 complex that demarcates the 5' end junctions of ssDNA gaps (not drawn). After DDC is activated for a prolonged period, Srs2 recruited to PCNA that demarcates the 3'

end junction flanking the ssDNA gaps can be sumoylated. Srs2 sumoylation level increases as Mec1 activation heightens and can result in more efficient RPA removal, leading to Mec1 downregulation.

Acknowledgments. We thank Drs. James Haber, Marco Foiani, Daniele Piccini, John Petrini for sharing antibodies, and Tzippora Chwat-Edelstein for critical reading of the manuscript. X.Z. is supported by National Institute of General Medical Sciences (NIGMS) grants R35GM145260.

Author contributions: All authors were involved in research design and data analyses, J. F., N. D., T. Y., and V. Y. performed research. J. F. and and X.Z. wrote the paper with all authors' input.

Competing interest statement: The authors declare no competing interests.

Supplemental Materials

Figure S1. *srs2* mutants examined for CPT sensitivity and interactions with *rfa1* mutant

(A) *srs2* mutants exhibit different levels of CPT sensitivity. *srs2-ΔPIM* showed slow growth on 8 µg/ml CPT. Sensitivity *srs2-SIM^{MUT}* toward CPT was seen at three CPT concentrations. *srs2-7AV* showed slow growth on media containing 4 and 8 µg/ml CPT. *srs2Δ* and *rfa1-zm2* are mutually suppressive for CPT sensitivity. Experiments are performed as in Figure 2C.

(B) *srs2-ΔPIM* confers better suppression of *rfa1-zm2's* CPT and MMS sensitivity than *srs2-3KR*. We note that mild suppression of *rfa1-zm2* by *srs2-3KR* was only seen at 0.03% MMS plates. Experiments are performed as in Figure 2C, and incubation times are noted. Dashed lines indicated removal of superfluous rows.

(C) *srs2-ΔPIM* suppresses *rfa1-t33* sensitivity toward MMS. Dashed lines indicated removal of superfluous rows.

Figure S2. *srs2-ΔPIM* and *slx4^{RIM}* are additively defective in DDC down-regulation

(A) The *srs2-ΔPIMΔ slx4^{RIM}* double mutant shows stronger CPT sensitivity than either single mutant. Experiments are performed as in Figure 2C.

(B) *srs2-ΔPIM* and *slx4^{RIM}* are additive for increasing the levels of active Rad53 when cells are treated with CPT. Experiments were conducted and quantifications are presented as those described in Figure 3A, except that three biological isolates are included.

(C) *srs2-ΔPIM* and *slx4^{RIM}* are additive for reducing the G1 cells exiting from G2/M arrest 2 hours post CPT treatment. Experiments were conducted and quantifications are presented as those described in Figure 3B, except that three biological isolates are included..

Figure S3. Confirmation of Srs2 sumoylation and Mec1-S1964 phosphorylation.

(A) Detection of Srs2 sumoylation. Protein extracts from asynchronous cells were bound to Ni-NTA beads and the elutes were subsequently examined by immunoblotting using anti-Srs2 antibody. Sumoylated Srs2 form was detected in wild-type cells expressing 8His-tagged yeast SUMO (Smt3) but not in cells lacking this fusion or in *srs2Δ* cells. Unmodified Srs2 showed unspecific Ni-NTA bead binding, thus detectable in cells containing Srs2 regardless of SUMO fusion.

(B) Detection of Mec1-S1964 phosphorylation. Cells were treated with CPT for 2 hours before immunoprecipitating Ddc2-myc was conducted. Ddc2 and the co- immunoprecipitated Mec1 were examined by immunoblotting. The phosphorylation at Mec1 Ser1964 site was detected by anti-Mec1-S1964-p antibody. This antibody also revealed an non-specific band (*). Cells containing untagged Ddc2 or the *mec1-S1964A* mutation were used as control.

Figure S4. Examination of Mec1-S964 phosphorylation.

(A) *mec1-S1964A* does not affect the CPT sensitivity of *srs2-3KR* or *srs2-3KR rfa1-zm2* cells Experiments were performed as in Figure 2C.

(B) The effects of *mec1-S1964E* on the CPT sensitivity of *srs2-3KR* and *srs2-ΔPIM* cells with or without *rfa1-zm2* cells. Experiments were performed as in Figure 2C.

(C) Mec1-S1964A or -S1964E does not affect Srs2 sumoylation. Experiments were performed as in Figure 4A. Mean values of three biological isolates per genotype are graphed with error bars representing SD. ns, not significant.

Table S1: Strains used in this study

All strains are derived from W1588-4C, a *RAD5* derivative of W303 (*MATa ade2-1 can1-100 ura3-1 his3-11,15, leu2-3, 112 trp1-1 rad5-535*). Only one strain is listed for each genotype, but at least two independent isolates of each genotype were used in the experiments.

Strain	Genotype	Source
X8665-12-22D	*MATa srs2-ΔPIM*	This study
X8198-15B	*srs2-SIM^{MUT}*	This study
G1114	*MATa srs2-7AV::HIS3*	(Saponaro et al., 2010)
X8650-2-1D	*MATa srs2-3KR::NAT*	This study
X8659-14A	*MATa srs2-2SA*	This study
G854	*MATα srs2-Δ(875-902)::HPH*	(Colavito et al., 2009)
X8047-1B	*MATα rfa1-zm2*	(Dhingra et al., 2021)
X8650-2C	*MATa srs2-3KR::NAT rfa1-zm2*	This study
X8666-35-6A	*MATa srs2-ΔPIM rfa1-zm2*	This study
X8210-2B	*MATa rfa1-t33*	(Dhingra et al., 2021)
X8745-2A	*MATa srs2-3KR::NAT rfa1-t33*	This study
X8743-13A	*MATα srs2-ΔPIM rfa1-t33*	This study
X8198-15A	*srs2-SIM^{MUT} rfa1-zm2*	This study
X8637-6B	*MATa srs2-7AV::HIS3 rfa1-zm2*	This study
X8137-10B	*MATa srs2-Δ875-902::HPH rfa1-zm2*	This study
X8660-4B	*MATα srs2-2SA rfa1-zm2*	This study
T1358-2	*MATa 8His-SMT3::TRP1*	Lab Collection
X8808-2D	*MATa srs2-ΔPIM 8His-SMT3::TRP1*	This study
X8795-9D	*MATa srs2-3KR::NAT 8His-SMT3::TRP1*	This study
X8807-6A	*MATa sml1Δ::URA3 8His-SMT3::TRP1*	This study
X8746-4D	*MATa sml1Δ::URA3 mec1Δ::TRP1 8His-SMT3::TRP1*	This study
X8807-7A	*MATa sml1Δ::URA3 rad53Δ::HIS3 8His-SMT3::TRP1*	This study
G461	*MATa 3FLAG-RAD53::LEU2*	J. Petrini
X9055-1D	*MATa DDC2-Myc18::HIS3*	This study
X9225-3A	*MATa mec1-S1964A*	This study
X9225-3C	*MATa mec1-S1964A rfa1-zm2*	This study
X9088-38C	*MATa mec1-S1964A srs2-ΔPIM*	This study
X9225-1B	*MATα mec1-S1964A srs2-ΔPIM rfa1-zm2*	This study
X8495-5D	*MATa rfa1-S178D*	This study
X8495-2D	*MATa srs2Δ::HIS3 rfa1-S178D*	This study
X8494-3B	*MATa rfa1-S178A*	This study
X8494-3A	*MATa srs2Δ::HIS3 rfa1-S178A*	This study
X8658-14-22D	*MATa rfa2-3SA*	This study
X8658-14-13C	*MATa srs2Δ::HIS3 rfa2-3SA*	This study
X8779-13D	*MATa rfa2-3SD*	This study
X8779-13B	*MATa srs2Δ rfa2-3SD*	This study
X9265-4D	*MATa SLX4-TAP::HIS3*	(Wan et al., 2019)
X9265-4A	*MATa srs2-ΔPIM SLX4-TAP::HIS3*	This study
X8956-7C	*MATa slx4^{RIM}-TAP::HIS3*	(Wan et al., 2019)
X8956-5D	*MATa srs2-ΔPIM slx4^{RIM}-TAP::HIS3*	This study
X9228-2D	*MATa mec1-S1964A srs2-3KR::NAT*	This study
X9228-5A	*MATα mec1-S1964A srs2-3KR::NAT rfa1-zm2*	This study
X9090-9C	*MATa mec1-S1964E*	This study
X9091-14A	*MATa mec1-S1964E rfa1-zm2*	This study
X9090-19A	*MATa mec1-S1964E srs2-ΔPIM*	This study
X9132-15B	*MATa mec1-S1964E srs2-ΔPIM rfa1-zm2*	This study

X9091-13A	*MATa mec1-S1964E srs2-3KR::NAT*	This study
X9132-10B	*MATα mec1-S1964A srs2-3KR::NAT rfa1-zm2*	This study
X9137-3B	*MATa mec1-S1964A 8His-SMT3::TRP1*	This study
X9136-2B	*MATa mec1-S1964E 8His-SMT3::TRP1*	This study

Reference:

Albuquerque, C. P., Yeung, E., Ma, S., Fu, T., Corbett, K. D., & Zhou, H. (2015). A Chemical and Enzymatic Approach to Study Site-Specific Sumoylation. *PLoS One*, *10*(12), e0143810. https://doi.org/10.1371/journal.pone.0143810

Antony, E., Tomko, E. J., Xiao, Q., Krejci, L., Lohman, T. M., & Ellenberger, T. (2009). Srs2 Disassembles Rad51 Filaments by a Protein-Protein Interaction Triggering ATP Turnover and Dissociation of Rad51 from DNA. *Molecular Cell*, *35*(1), 105-115. https://doi.org/10.1016/j.molcel.2009.05.026

Bronstein, A., Bramson, S., Shemesh, K., Liefshitz, B., & Kupiec, M. (2018). Tight Regulation of Srs2 Helicase Activity Is Crucial for Proper Functioning of DNA Repair Mechanisms. *G3 (Bethesda)*, *8*(5), 1615-1626. https://doi.org/10.1534/g3.118.200181

Chen, S.-h., Albuquerque, C. P., Liang, J., Suhandynata, R. T., & Zhou, H. (2010). A Proteome-wide Analysis of Kinase-Substrate Network in the DNA Damage Response. *Journal of Biological Chemistry*, *285*(17), 12803-12812. https://doi.org/10.1074/jbc.M110.106989

Chiolo, I., Carotenuto, W., Maffioletti, G., Petrini, J. H., Foiani, M., & Liberi, G. (2005). Srs2 and Sgs1 DNA helicases associate with Mre11 in different subcomplexes following checkpoint activation and CDK1-mediated Srs2 phosphorylation. *Mol Cell Biol*, *25*(13), 5738-5751. https://doi.org/10.1128/MCB.25.13.5738-5751.2005

Chung, I., & Zhao, X. (2015). DNA break-induced sumoylation is enabled by collaboration between a SUMO ligase and the ssDNA-binding complex RPA. *Genes Dev*, *29*(15), 1593-1598. https://doi.org/10.1101/gad.265058.115

Colavito, S., Macris-Kiss, M., Seong, C., Gleeson, O., Greene, E. C., Klein, H. L., Krejci, L., & Sung, P. (2009). Functional significance of the Rad51-Srs2 complex in Rad51 presynaptic filament disruption. *Nucleic Acids Res*, *37*(20), 6754-6764. https://doi.org/10.1093/nar/gkp748

Cremona, C. A., Sarangi, P., Yang, Y., Hang, L. E., Rahman, S., & Zhao, X. (2012). Extensive DNA damage-induced sumoylation contributes to replication and repair and acts in addition to the mec1 checkpoint. *Mol Cell*, *45*(3), 422-432. https://doi.org/10.1016/j.molcel.2011.11.028

Deng, S. K., Gibb, B., de Almeida, M. J., Greene, E. C., & Symington, L. S. (2014). RPA antagonizes microhomology-mediated repair of DNA double-strand breaks. *Nat Struct Mol Biol*, *21*(4), 405-412. https://doi.org/10.1038/nsmb.2786

Dhingra, N., Kuppa, S., Wei, L., Pokhrel, N., Baburyan, S., Meng, X., Antony, E., & Zhao, X. (2021). The Srs2 helicase dampens DNA damage checkpoint by recycling RPA from chromatin. *Proc Natl Acad Sci U S A*, *118*(8). https://doi.org/10.1073/pnas.2020185118

DiCarlo, J. E., Norville, J. E., Mali, P., Rios, X., Aach, J., & Church, G. M. (2013). Genome engineering in Saccharomyces cerevisiae using CRISPR-Cas systems. *Nucleic Acids Research*, *41*(7), 4336-4343. https://doi.org/10.1093/nar/gkt135

Faca, V. M., Sanford, E. J., Tieu, J., Comstock, W., Gupta, S., Marshall, S., Yu, H., & Smolka, M. B. (2020). Maximized quantitative phosphoproteomics allows high confidence dissection of the DNA damage signaling network. *Scientific Reports*, *10*(1), 18056. https://doi.org/10.1038/s41598-020-74939-4

Fan, J., & Pavletich, N. P. (2012). Structure and conformational change of a replication protein A heterotrimer bound to ssDNA. *Genes Dev*, *26*(20), 2337-2347. https://doi.org/10.1101/gad.194787.112

Fan, L., Zhang, W., Rybchuk, J., Luo, Y., & Xiao, W. (2023). Genetic Dissection of Budding Yeast PCNA Mutations Responsible for the Regulated Recruitment of Srs2 Helicase. *mBio*, *14*(2), e00315-00323. https://doi.org/10.1128/mbio.00315-23

Fiorani, S., Mimun, G., Caleca, L., Piccini, D., & Pellicioli, A. (2008). Characterization of the activation domain of the Rad53 checkpoint kinase. *Cell Cycle*, *7*(4), 493-499. https://doi.org/10.4161/cc.7.4.5323

Hormeno, S., Wilkinson, O. J., Aicart-Ramos, C., Kuppa, S., Antony, E., Dillingham, M. S., & Moreno-Herrero, F. (2022). Human HELB is a processive motor protein that catalyzes RPA clearance

from single-stranded DNA. *Proceedings of the National Academy of Sciences*, *119*(15), e2112376119. https://doi.org/10.1073/pnas.2112376119

Jenkins, T., Northall, S. J., Ptchelkine, D., Lever, R., Cubbon, A., Betts, H., Taresco, V., Cooper, C. D. O., McHugh, Peter J., Soultanas, P., & Bolt, E. L. (2021). The HelQ human DNA repair helicase utilizes a PWI-like domain for DNA loading through interaction with RPA, triggering DNA unwinding by the HelQ helicase core. *NAR Cancer*, *3*(1), zcaa043. https://doi.org/10.1093/narcan/zcaa043

Kolesar, P., Altmannova, V., Silva, S., Lisby, M., & Krejci, L. (2016). Pro-recombination Role of Srs2 Protein Requires SUMO (Small Ubiquitin-like Modifier) but Is Independent of PCNA (Proliferating Cell Nuclear Antigen) Interaction. *J Biol Chem*, *291*(14), 7594-7607. https://doi.org/10.1074/jbc.M115.685891

Kolesar, P., Sarangi, P., Altmannova, V., Zhao, X., & Krejci, L. (2012). Dual roles of the SUMO-interacting motif in the regulation of Srs2 sumoylation. *Nucleic Acids Res*, *40*(16), 7831-7843. https://doi.org/10.1093/nar/gks484

Krejci, L., Van Komen, S., Li, Y., Villemain, J., Reddy, M. S., Klein, H., Ellenberger, T., & Sung, P. (2003). DNA helicase Srs2 disrupts the Rad51 presynaptic filament. *Nature*, *423*(6937), 305-309. https://doi.org/10.1038/nature01577

Lanz, M. C., Dibitetto, D., & Smolka, M. B. (2019). DNA damage kinase signaling: checkpoint and repair at 30 years. *EMBO J*, *38*(18), e101801. https://doi.org/10.15252/embj.2019101801

Lanz, M. C., Yugandhar, K., Gupta, S., Sanford, E. J., Faça, V. M., Vega, S., Joiner, A. M. N., Fromme, J. C., Yu, H., & Smolka, M. B. (2021). In-depth and 3-dimensional exploration of the budding yeast phosphoproteome. *EMBO reports*, *22*(2), e51121. https://doi.org/10.15252/embr.202051121

Li, S., Xu, Z., Xu, J., Zuo, L., Yu, C., Zheng, P., Gan, H., Wang, X., Li, L., Sharma, S., Chabes, A., Li, D., Wang, S., Zheng, S., Li, J., Chen, X., Sun, Y., Xu, D., Han, J., . . . Li, Q. (2018). Rtt105 functions as a chaperone for replication protein A to preserve genome stability. *EMBO J*, *37*(17). https://doi.org/10.15252/embj.201899154

Maréchal, A., & Zou, L. (2015). RPA-coated single-stranded DNA as a platform for post-translational modifications in the DNA damage response. *Cell Research*, *25*(1), 9-23. https://doi.org/10.1038/cr.2014.147

Memisoglu, G., Lanz, M. C., Eapen, V. V., Jordan, J. M., Lee, K., Smolka, M. B., & Haber, J. E. (2019). Mec1(ATR) Autophosphorylation and Ddc2(ATRIP) Phosphorylation Regulates DNA Damage Checkpoint Signaling. *Cell Rep*, *28*(4), 1090-1102 e1093. https://doi.org/10.1016/j.celrep.2019.06.068

Moldovan, G.L., Pfander, B., & Jentsch, S. (2007). PCNA, the Maestro of the Replication Fork. *Cell*, *129*(4), 665-679. https://doi.org/10.1016/j.cell.2007.05.003

Niu, H., & Klein, H. L. (2017). Multifunctional roles of Saccharomyces cerevisiae Srs2 protein in replication, recombination and repair. *FEMS Yeast Res*, *17*(2). https://doi.org/10.1093/femsyr/fow111

Ohouo, P. Y., Bastos De Oliveira, F. M., Liu, Y., Ma, C. J., & Smolka, M. B. (2013). DNA-repair scaffolds dampen checkpoint signalling by counteracting the adaptor Rad9. *Nature*, *493*(7430), 120-124. https://doi.org/10.1038/nature11658

Papouli, E., Chen, S., Davies, A. A., Huttner, D., Krejci, L., Sung, P., & Ulrich, H. D. (2005). Crosstalk between SUMO and ubiquitin on PCNA is mediated by recruitment of the helicase Srs2p. *Mol Cell*, *19*(1), 123-133. https://doi.org/10.1016/j.molcel.2005.06.001

Pellicioli, A., Lee, S. E., Lucca, C., Foiani, M., & Haber, J. E. (2001). Regulation of Saccharomyces Rad53 Checkpoint Kinase during Adaptation from DNA Damage–Induced G2/M Arrest. *Molecular Cell*, *7*(2), 293-300. https://doi.org/10.1016/S1097-2765(01)00177-0

Pfander, B., Moldovan, G. L., Sacher, M., Hoege, C., & Jentsch, S. (2005). SUMO-modified PCNA recruits Srs2 to prevent recombination during S phase. *Nature*, *436*(7049), 428-433. https://doi.org/10.1038/nature03665

Psakhye, I., & Jentsch, S. (2012). Protein group modification and synergy in the SUMO pathway as exemplified in DNA repair. *Cell*, *151*(4), 807-820. https://doi.org/10.1016/j.cell.2012.10.021

Regan-Mochrie, G., Hoggard, T., Bhagwat, N., Lynch, G., Hunter, N., Remus, D., Fox, C. A., & Zhao, X. (2022). Yeast ORC sumoylation status fine-tunes origin licensing. *Genes & Development*. https://doi.org/10.1101/gad.349610.122

Sanchez, Y., Bachant, J., Wang, H., Hu, F., Liu, D., Tetzlaff, M., & Elledge, S. J. (1999). Control of the DNA Damage Checkpoint by Chk1 and Rad53 Protein Kinases Through Distinct Mechanisms. *Science*, *286*(5442), 1166-1171. https://doi.org/10.1126/science.286.5442.1166

Saponaro, M., Callahan, D., Zheng, X., Krejci, L., Haber, J. E., Klein, H. L., & Liberi, G. (2010). Cdk1 targets Srs2 to complete synthesis-dependent strand annealing and to promote recombinational repair. *PLoS Genet*, *6*(2), e1000858. https://doi.org/10.1371/journal.pgen.1000858

Seeber, A., Hegnauer, A. M., Hustedt, N., Deshpande, I., Poli, J., Eglinger, J., Pasero, P., Gut, H., Shinohara, M., Hopfner, K.-P., Shimada, K., & Gasser, S. M. (2016). RPA Mediates Recruitment of MRX to Forks and Double-Strand Breaks to Hold Sister Chromatids Together. *Molecular Cell*, *64*(5), 951-966. https://doi.org/10.1016/j.molcel.2016.10.032

Shorrocks, A.-M. K., Jones, S. E., Tsukada, K., Morrow, C. A., Belblidia, Z., Shen, J., Vendrell, I., Fischer, R., Kessler, B. M., & Blackford, A. N. (2021). The Bloom syndrome complex senses RPA-coated single-stranded DNA to restart stalled replication forks. *Nature Communications*, *12*(1), 585. https://doi.org/10.1038/s41467-020-20818-5

Smith, J., & Rothstein, R. (1995). A Mutation in the Gene Encoding the *Saccharomyces cerevisiae* Single-Stranded DNA-Binding Protein Rfa1 Stimulates a *RAD52* -Independent Pathway for Direct-Repeat Recombination. *Molecular and Cellular Biology*, *15*(3), 1632-1641. https://doi.org/10.1128/MCB.15.3.1632

Ulrich, H. D., & Davies, A. A. (2009). In vivo detection and characterization of sumoylation targets in Saccharomyces cerevisiae. *Methods in molecular biology (Clifton, N.J.)*, *497*, 81-103. https://doi.org/10.1007/978-1-59745-566-4_6

Umezu, K., Sugawara, N., Chen, C., Haber, J. E., & Kolodner, R. D. (1998). Genetic Analysis of Yeast RPA1 Reveals Its Multiple Functions in DNA Metabolism. *Genetics*, *148*(3), 989-1005. https://doi.org/10.1093/genetics/148.3.989

Usui, T., Foster, S. S., & Petrini, J. H. J. (2009). Maintenance of the DNA-Damage Checkpoint Requires DNA-Damage-Induced Mediator Protein Oligomerization. *Molecular Cell*, *33*(2), 147-159. https://doi.org/10.1016/j.molcel.2008.12.022

Wan, B., Wu, J., Meng, X., Lei, M., & Zhao, X. (2019). Molecular Basis for Control of Diverse Genome Stability Factors by the Multi-BRCT Scaffold Rtt107. *Mol Cell*, *75*(2), 238-251 e235. https://doi.org/10.1016/j.molcel.2019.05.035

Wang, H., Liu, D., Wang, Y., Qin, J., & Elledge, S. J. (2001). Pds1 phosphorylation in response to DNA damage is essential for its DNA damage checkpoint function. *Genes & Development*, *15*(11), 1361-1372. https://doi.org/10.1101/gad.893201

Waterman, D. P., Haber, J. E., & Smolka, M. B. (2020). Checkpoint Responses to DNA Double-Strand Breaks. *Annual Review of Biochemistry*, *89*(1), 103-133. https://doi.org/10.1146/annurev-biochem-011520-104722

Zhao, X., & Blobel, G. (2005). A SUMO ligase is part of a nuclear multiprotein complex that affects DNA repair and chromosomal organization. *Proc Natl Acad Sci U S A*, *102*(13), 4777-4782. https://doi.org/10.1073/pnas.0500537102

Zhao, X., & Rothstein, R. (2002). The Dun1 checkpoint kinase phosphorylates and regulates the ribonucleotide reductase inhibitor Sml1. *Proc Natl Acad Sci U S A*, *99*(6), 3746-3751. https://doi.org/10.1073/pnas.062502299

Zou, L., & Elledge, S. J. (2003). Sensing DNA Damage Through ATRIP Recognition of RPA-ssDNA Complexes. *Science*, *300*(5625), 1542-1548. https://doi.org/10.1126/science.1083430

Fig. 1

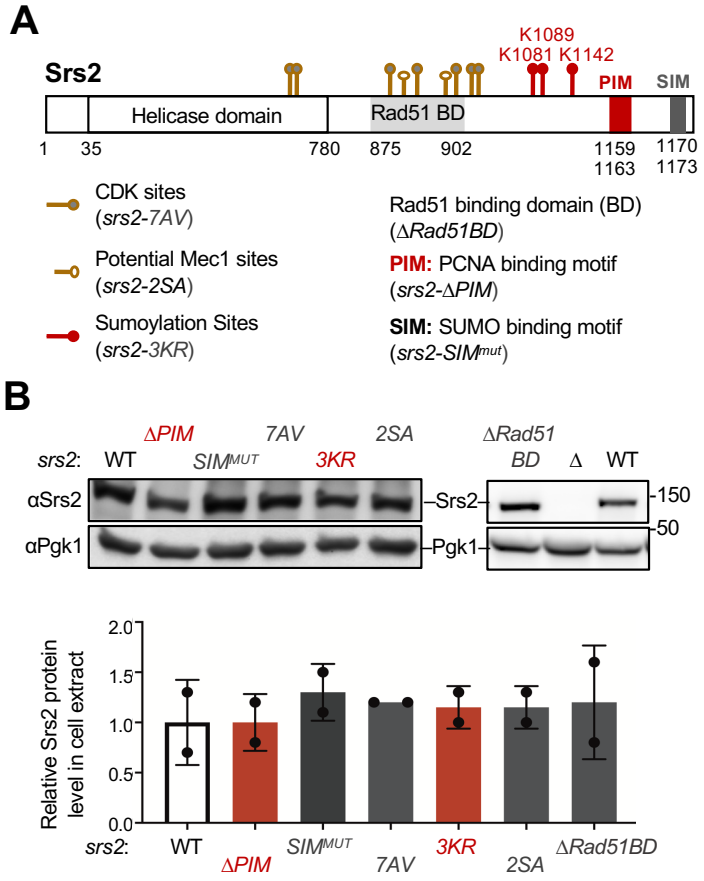
A
Srs2
K1089
K1081 K1142
PIM
SIM
Helicase domain
Rad51 BD
1
35
780
875
902
1159
1163
1170
1173
CDK sites
(srs2-7AV)
Potential Mec1 sites
(srs2-2SA)
Sumoylation Sites
(srs2-3KR)
Rad51 binding domain (BD)
(ΔRad51BD)
PIM: PCNA binding motif
(srs2-ΔPIM)
SIM: SUMO binding motif
(srs2-SIMmut)
B
srs2:
WT
ΔPIM
SIMMUT
7AV
3KR
2SA
ΔRad51 BD
Δ
WT
αSrs2
αPgk1
Srs2
Pgk1
150
50
Relative Srs2 protein level in cell extract
2.0
1.5
1.0
0.5
0.0
srs2:
WT
ΔPIM
SIMMUT
7AV
3KR
2SA
ΔRad51BD

Fig. 2

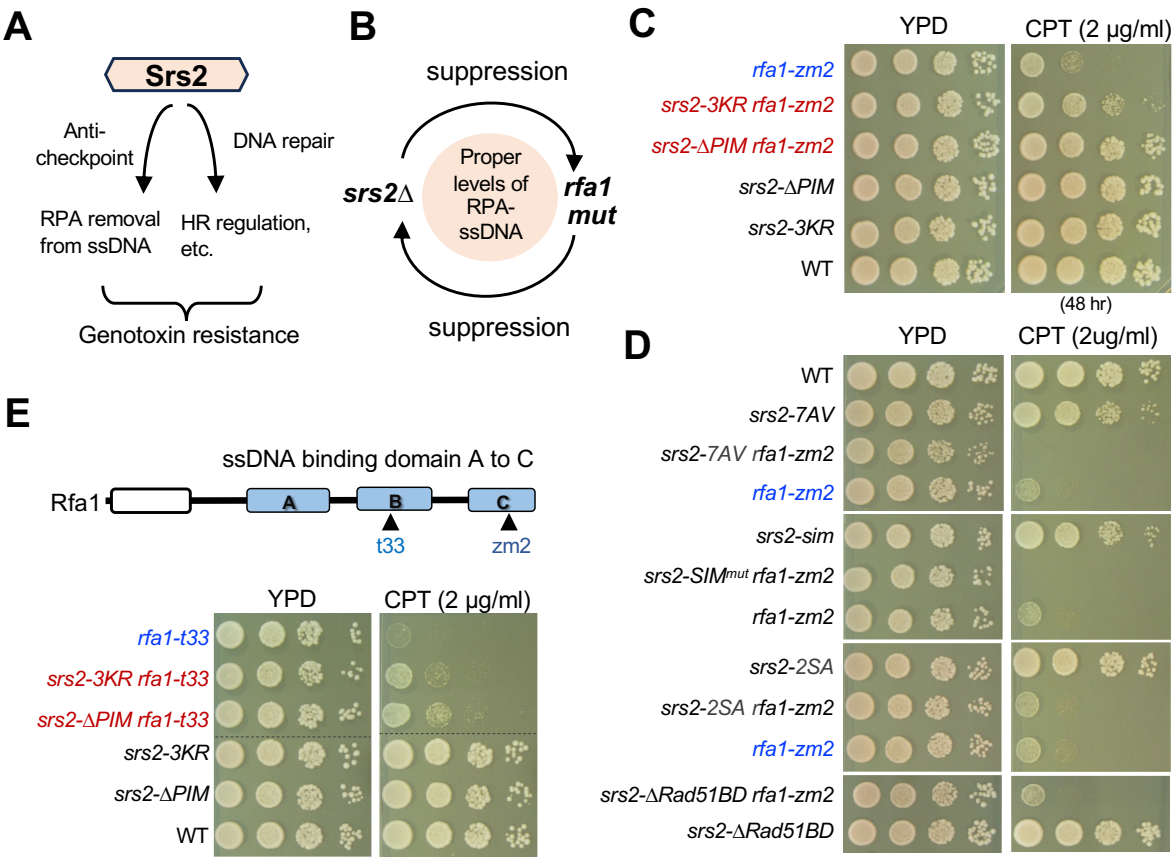
A
Srs2
Anti-checkpoint
DNA repair
RPA removal from ssDNA
HR regulation, etc.
Genotoxin resistance
B
suppression
srs2Δ
Proper levels of RPA-ssDNA
rfa1 mut
suppression
C
YPD
CPT (2 μg/ml)
rfa1-zm2
srs2-3KR rfa1-zm2
srs2-ΔPIM rfa1-zm2
srs2-ΔPIM
srs2-3KR
WT
(48 hr)
D
YPD
CPT (2ug/ml)
WT
srs2-7AV
srs2-7AV rfa1-zm2
rfa1-zm2
srs2-sim
srs2-SIMmut rfa1-zm2
rfa1-zm2
srs2-2SA
srs2-2SA rfa1-zm2
rfa1-zm2
srs2-ΔRad51BD rfa1-zm2
srs2-ΔRad51BD
E
ssDNA binding domain A to C
Rfa1
A
B
C
t33
zm2
YPD
CPT (2 μg/ml)
rfa1-t33
srs2-3KR rfa1-t33
srs2-ΔPIM rfa1-t33
srs2-3KR
srs2-ΔPIM
WT

Fig. 3

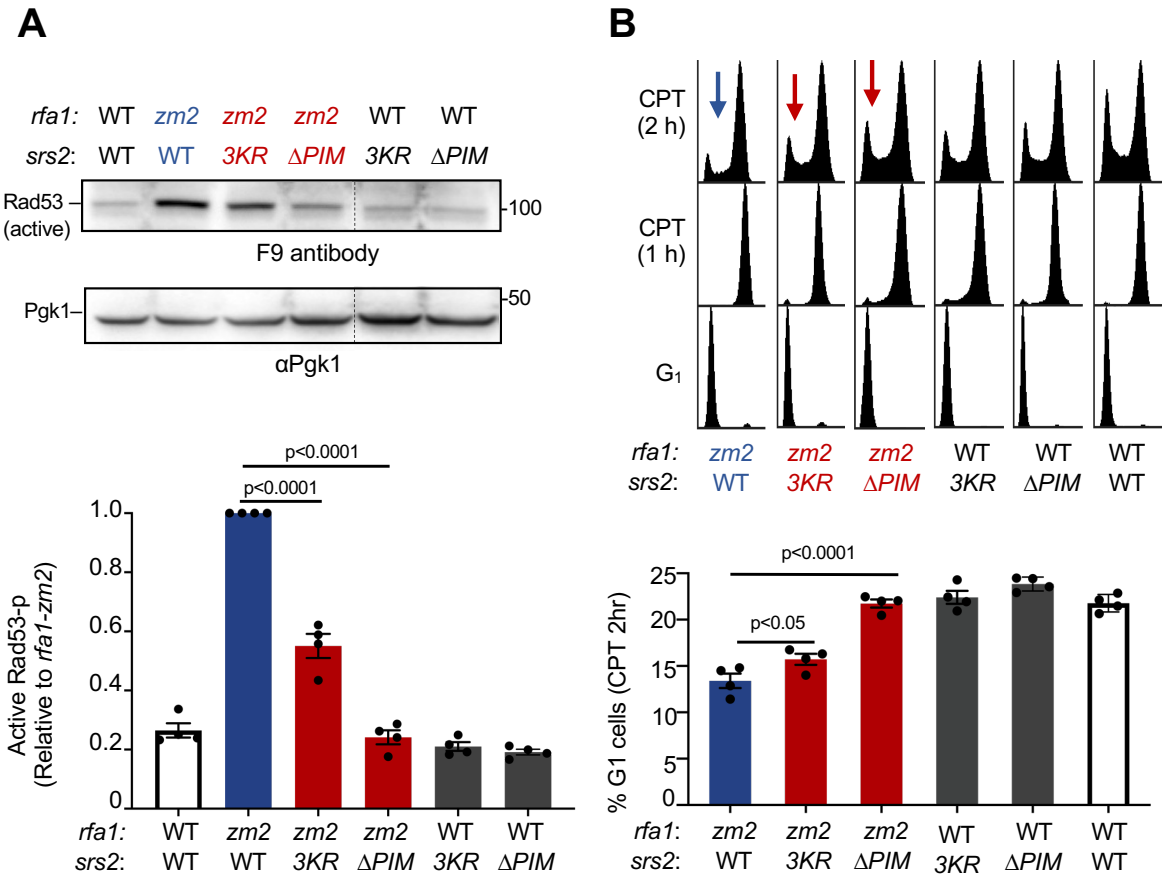
A
rfa1: WT zm2 zm2 zm2 WT WT
srs2: WT WT 3KR ΔPIM 3KR ΔPIM
Rad53 (active)
100
F9 antibody
Pgk1
50
αPgk1
p<0.0001
p<0.0001
Active Rad53-p (Relative to rfa1-zm2)
1.0
0.8
0.6
0.4
0.2
0
rfa1: WT zm2 zm2 zm2 WT WT
srs2: WT WT 3KR ΔPIM 3KR ΔPIM
B
CPT (2 h)
CPT (1 h)
G1
rfa1: zm2 zm2 zm2 WT WT WT
srs2: WT 3KR ΔPIM 3KR ΔPIM WT
p<0.0001
p<0.05
% G1 cells (CPT 2hr)
25
20
15
10
5
0
rfa1: zm2 zm2 zm2 WT WT WT
srs2: WT 3KR ΔPIM 3KR ΔPIM WT

Fig. 4

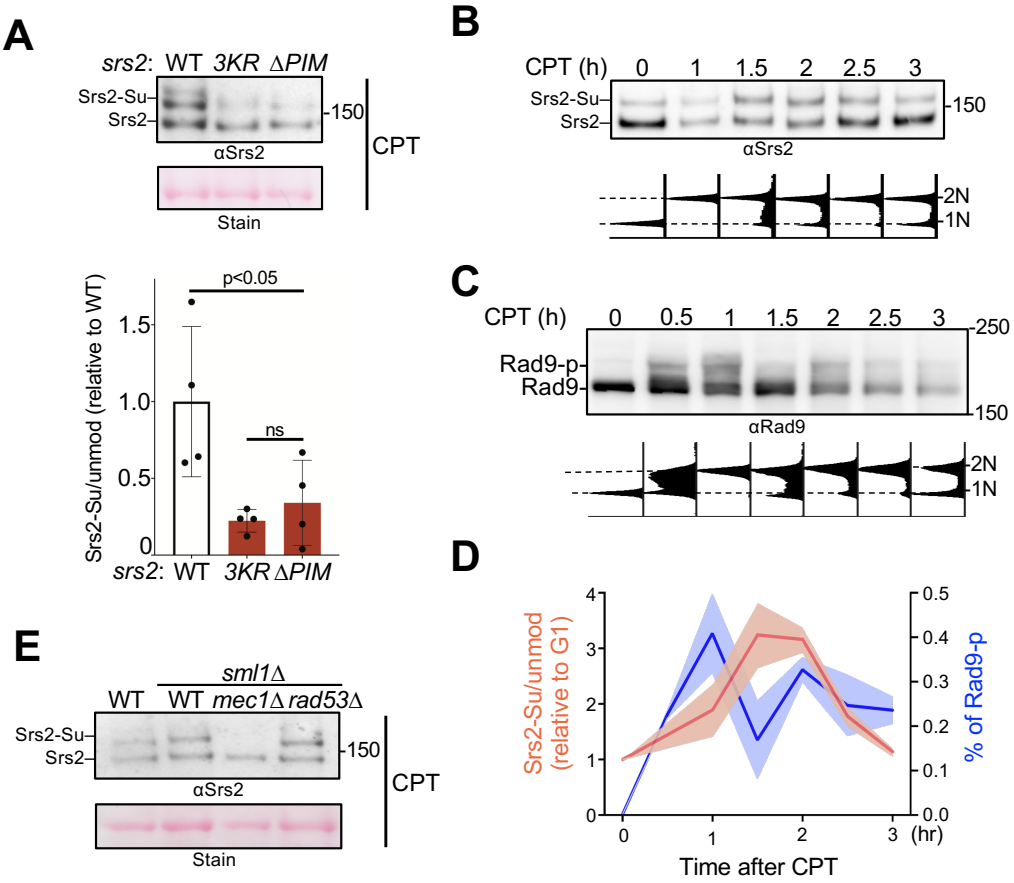
A
srs2: WT 3KR ΔPIM
Srs2-Su
Srs2
150
αSrs2
CPT
Stain
p<0.05
ns
Srs2-Su/unmod (relative to WT)
1.5
1.0
0.5
0
srs2: WT 3KR ΔPIM
B
CPT (h) 0 1 1.5 2 2.5 3
Srs2-Su
Srs2
150
αSrs2
2N
1N
C
CPT (h) 0 0.5 1 1.5 2 2.5 3
250
Rad9-p
Rad9
150
αRad9
2N
1N
D
Srs2-Su/unmod (relative to G1)
% of Rad9-p
Time after CPT
(hr)
E
sml1Δ
WT WT mec1Δ rad53Δ
Srs2-Su
Srs2
150
αSrs2
CPT
Stain

Fig. 5

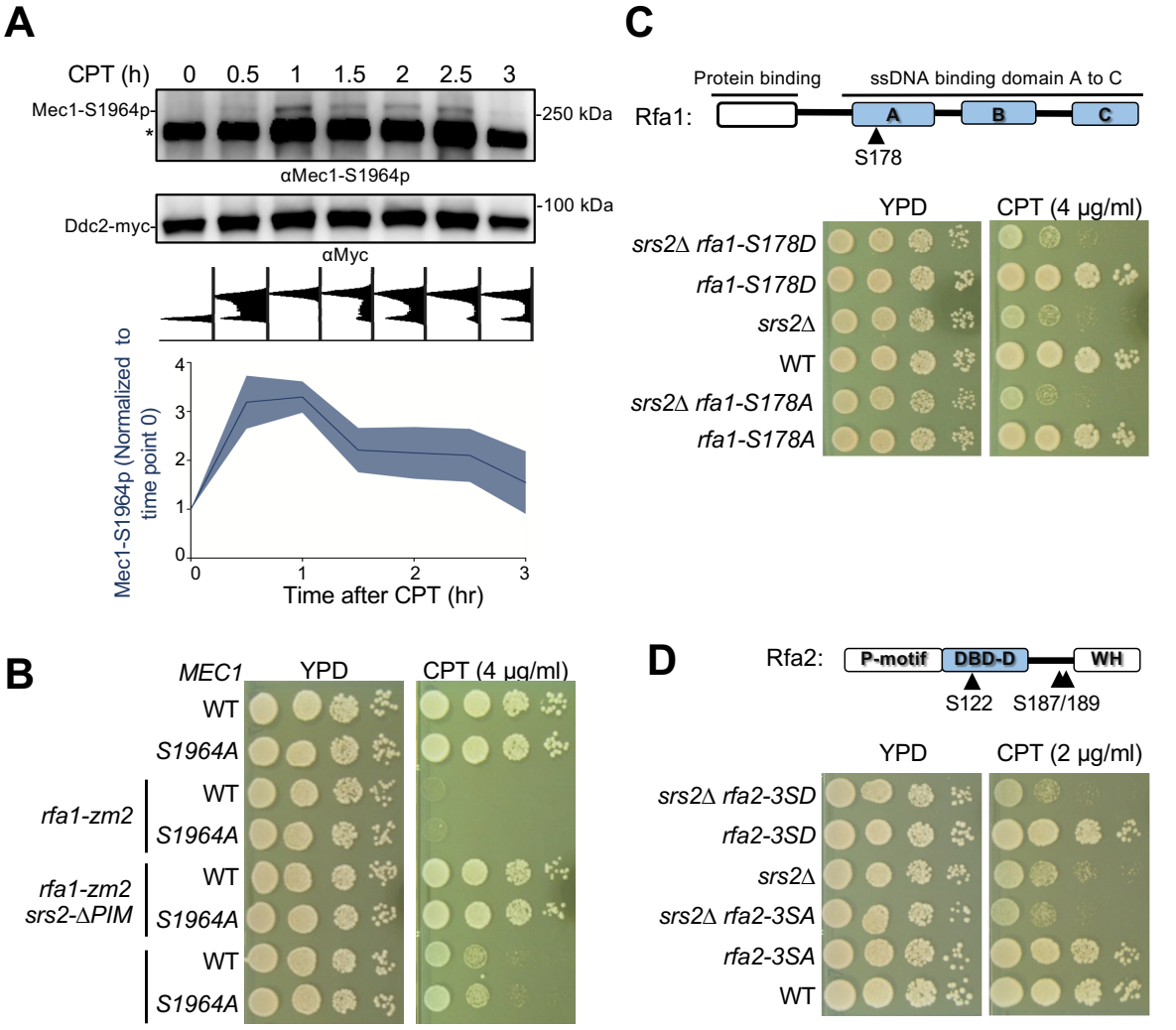
A
CPT (h) 0 0.5 1 1.5 2 2.5 3
Mec1-S1964p
*
250 kDa
αMec1-S1964p
Ddc2-myc
100 kDa
αMyc
Mec1-S1964p (Normalized to time point 0)
Time after CPT (hr)
B
MEC1
YPD
CPT (4 μg/ml)
WT
S1964A
rfa1-zm2
rfa1-zm2 srs2-ΔPIM
C
Protein binding
ssDNA binding domain A to C
Rfa1:
A
B
C
S178
srs2Δ rfa1-S178D
rfa1-S178D
srs2Δ
WT
srs2Δ rfa1-S178A
rfa1-S178A
D
Rfa2:
P-motif
DBD-D
WH
S122
S187/189
CPT (2 μg/ml)
srs2Δ rfa2-3SD
rfa2-3SD
srs2Δ
srs2Δ rfa2-3SA
rfa2-3SA
WT

Fig. 6

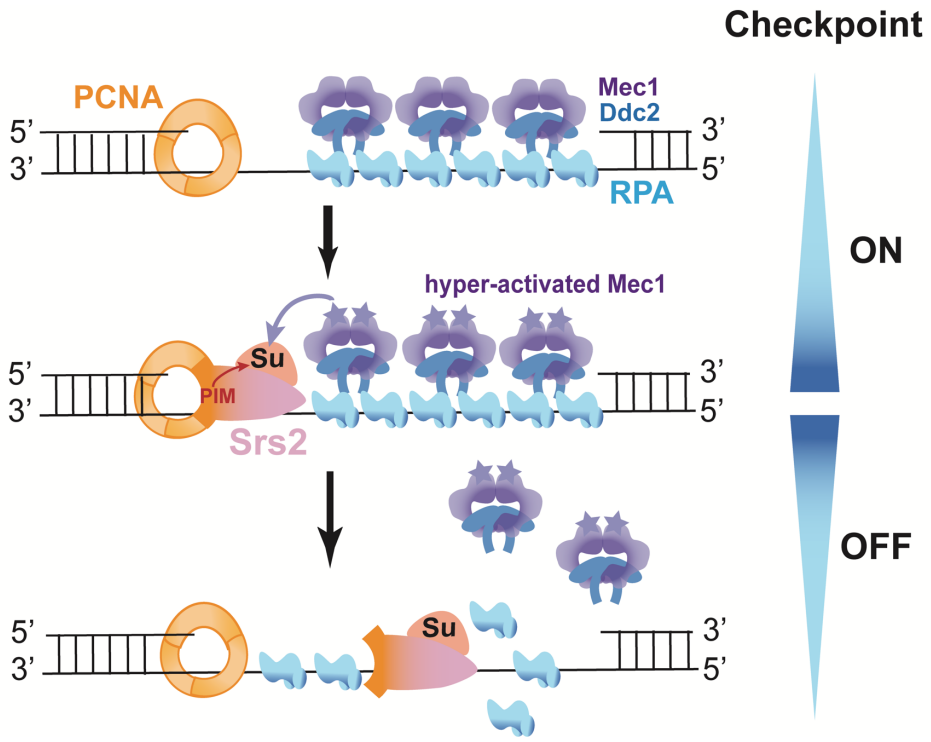
Checkpoint
PCNA
Mec1
Ddc2
5'
3'
3'
5'
RPA
ON
hyper-activated Mec1
Su
PIM
Srs2
5'
3'
3'
5'
OFF
Su
5'
3'
3'
5'

Figure S1

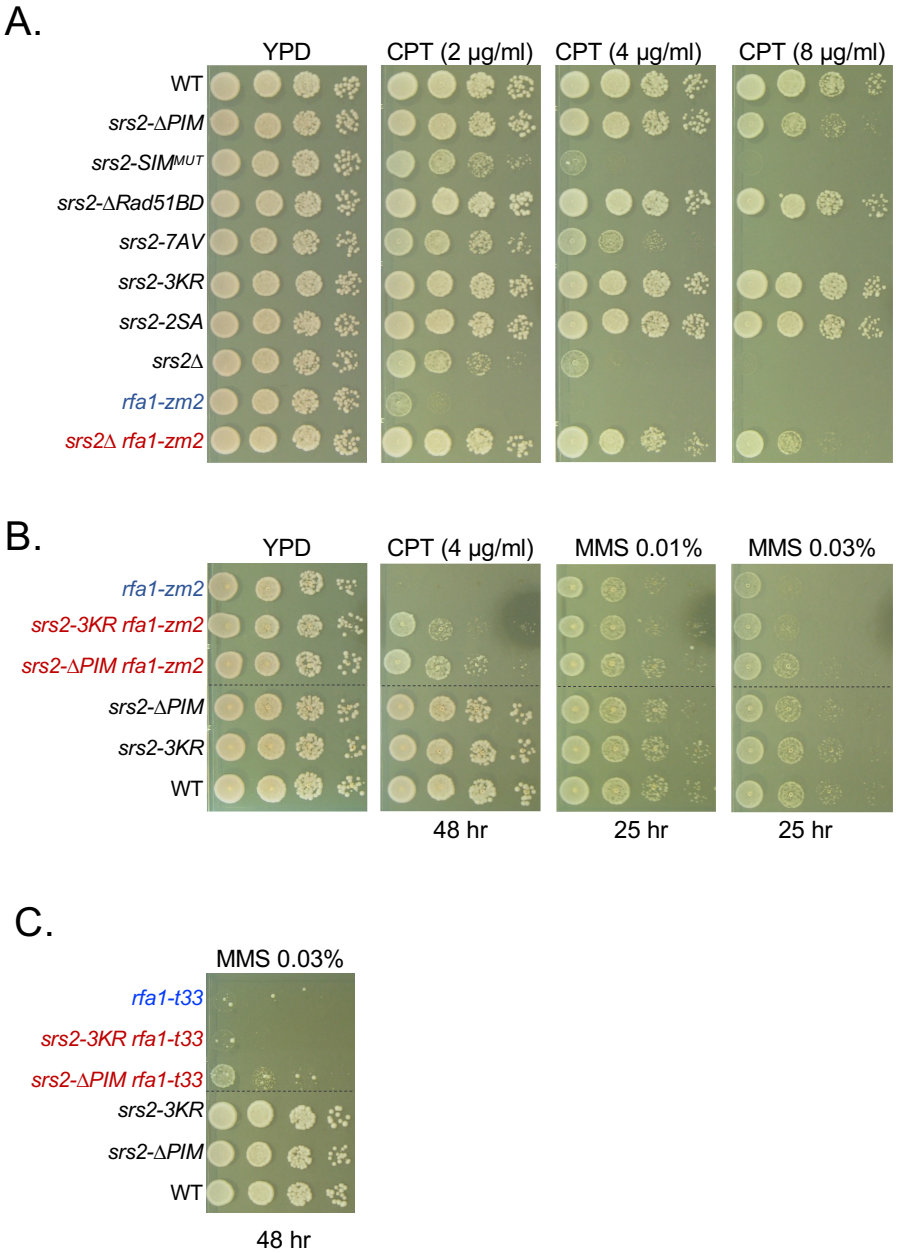
A.
YPD
CPT (2 µg/ml)
CPT (4 µg/ml)
CPT (8 µg/ml)
WT
srs2-ΔPIM
srs2-SIMMUT
srs2-ΔRad51BD
srs2-7AV
srs2-3KR
srs2-2SA
srs2Δ
rfa1-zm2
srs2Δ rfa1-zm2
B.
YPD
CPT (4 µg/ml)
MMS 0.01%
MMS 0.03%
rfa1-zm2
srs2-3KR rfa1-zm2
srs2-ΔPIM rfa1-zm2
srs2-ΔPIM
srs2-3KR
WT
48 hr
25 hr
25 hr
C.
MMS 0.03%
rfa1-t33
srs2-3KR rfa1-t33
srs2-ΔPIM rfa1-t33
srs2-3KR
srs2-ΔPIM
WT
48 hr

Figure S2

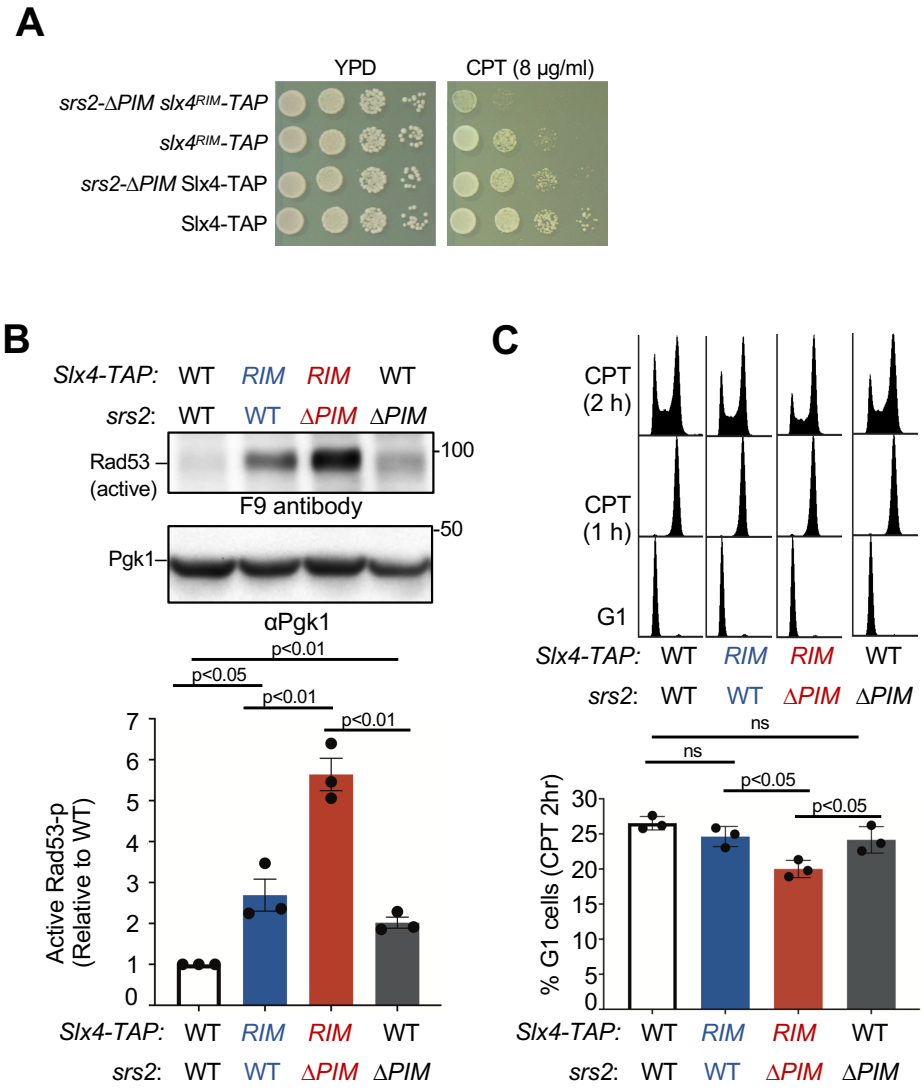
A
YPD
CPT (8 µg/ml)
srs2-ΔPIM slx4RIM-TAP
slx4RIM-TAP
srs2-ΔPIM Slx4-TAP
Slx4-TAP
B
Slx4-TAP: WT RIM RIM WT
srs2: WT WT ΔPIM ΔPIM
Rad53 (active)
100
F9 antibody
Pgk1
50
αPgk1
p<0.01
p<0.05
p<0.01
p<0.01
Active Rad53-p (Relative to WT)
0
1
2
3
4
5
6
7
Slx4-TAP: WT RIM RIM WT
srs2: WT WT ΔPIM ΔPIM
C
CPT (2 h)
CPT (1 h)
G1
Slx4-TAP: WT RIM RIM WT
srs2: WT WT ΔPIM ΔPIM
ns
ns
p<0.05
p<0.05
% G1 cells (CPT 2hr)
0
5
10
15
20
25
30
Slx4-TAP: WT RIM RIM WT
srs2: WT WT ΔPIM ΔPIM

Figure S3

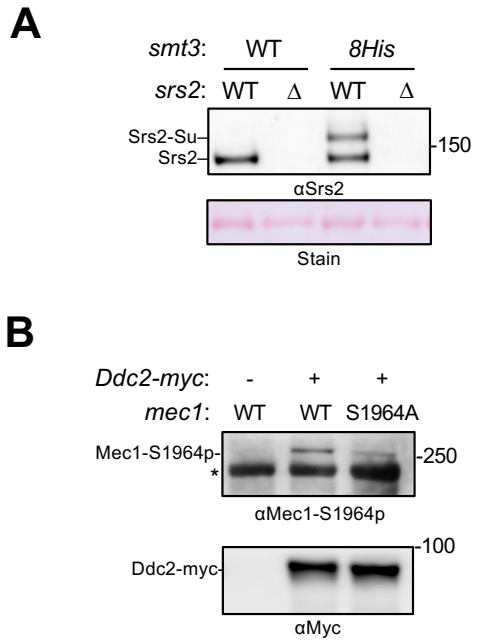
A
smt3: WT 8His
srs2: WT Δ WT Δ
Srs2-Su
Srs2
150
αSrs2
Stain
B
Ddc2-myc: - + +
mec1: WT WT S1964A
Mec1-S1964p
*
250
αMec1-S1964p
100
Ddc2-myc
αMyc

Figure S4

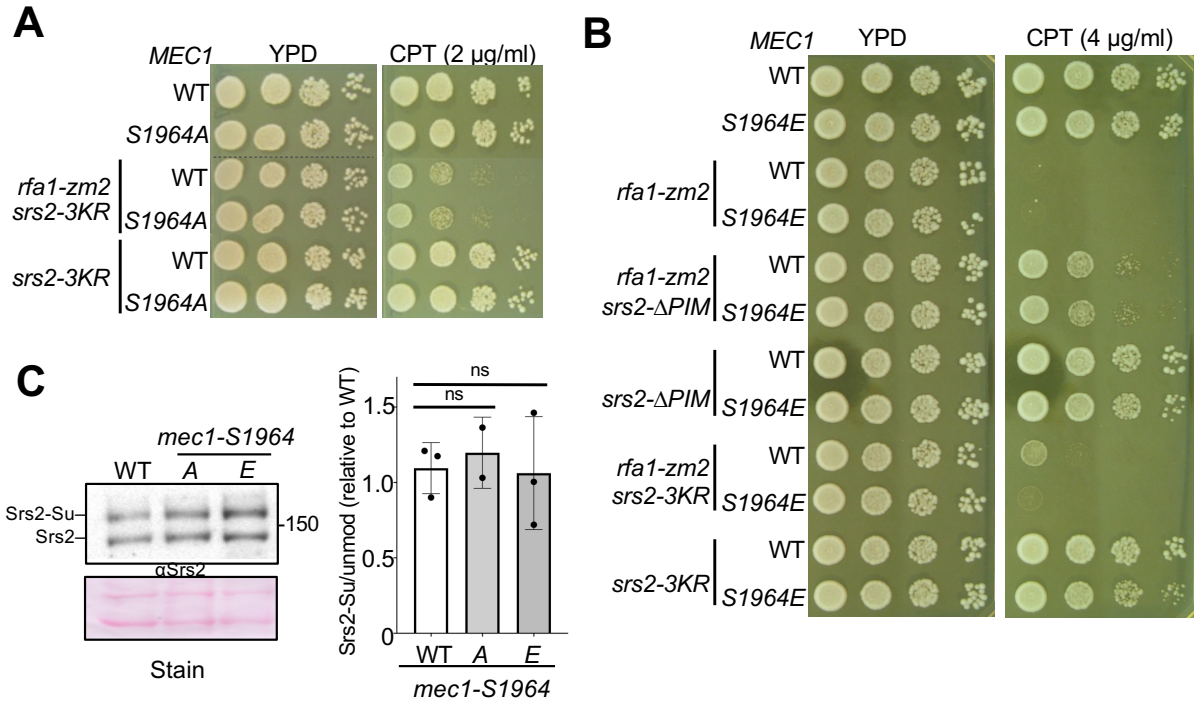
A
MEC1
YPD
CPT (2 µg/ml)
WT
S1964A
rfa1-zm2
srs2-3KR
WT
S1964A
srs2-3KR
WT
S1964A
B
MEC1
YPD
CPT (4 µg/ml)
WT
S1964E
rfa1-zm2
WT
S1964E
rfa1-zm2
srs2-ΔPIM
WT
S1964E
srs2-ΔPIM
WT
S1964E
rfa1-zm2
srs2-3KR
WT
S1964E
srs2-3KR
WT
S1964E
C
mec1-S1964
WT
A
E
Srs2-Su
Srs2
150
αSrs2
Stain
ns
ns
Srs2-Su/unmod (relative to WT)
1.5
1.0
0.5
0
WT
A
E
mec1-S1964